IOP Publishing J. Phys. Complex. 5 (2024) 015017 https://doi.org/10.1088/2632-072X/ad2698

Journal of Physics: Complexity

OPEN ACCESS

RECEIVED
16 March 2023

REVISED
11 December 2023

ACCEPTED FOR PUBLICATION
6 February 2024

PUBLISHED
6 March 2024

PAPER

Local sign stability and its implications for spectra of sparse random graphs and stability of ecosystems

Pietro Valigi[1,*], **Izaak Neri**[2] and **Chiara Cammarota**[1,3]

[1] Department of Physics, Sapienza University of Rome, P.le Aldo Moro 5, Rome 00185, Italy
[2] Department of Mathematics, King's College London, Strand, London WC2R 2LS, United Kingdom
[3] INFN: Istituto Nazionale di Fisica Nucleare, Sezione di Roma I, P.le Aldo Moro 5, Rome 00185, Italy
[*] Author to whom any correspondence should be addressed.

E-mail: pietro.valigi@uniroma1.it, izaak.neri@kcl.ac.uk and chiara.cammarota@uniroma1.it

Keywords: random matrices, sparse random graphs, complex dynamical systems, linear stability, sparse ecosystems

Abstract

We study the spectral properties of sparse random graphs with different topologies and type of interactions, and their implications on the stability of complex systems, with particular attention to ecosystems. Specifically, we focus on the behaviour of the leading eigenvalue in different type of random matrices (including interaction matrices and Jacobian-like matrices), relevant for the assessment of different types of dynamical stability. By comparing numerical results on Erdős–Rényi and Husimi graphs with sign-antisymmetric interactions or mixed sign patterns, we propose a sufficient criterion, called *strong local sign stability*, for stability not to be affected by system size, as traditionally implied by the complexity-stability trade-off in conventional models of random matrices. The criterion requires sign-antisymmetric or unidirectional interactions and a local structure of the graph such that the number of cycles of finite length do not increase with the system size. Note that the last requirement is stronger than the classical local tree-like condition, which we associate to the less stringent definition of *local sign stability*, also defined in the paper. In addition, for strong local sign stable graphs which show stability to linear perturbations irrespectively of system size, we observe that the leading eigenvalue can undergo a transition from being real to acquiring a nonnull imaginary part, which implies a dynamical transition from nonoscillatory to oscillatory linear response to perturbations. Lastly, we ascertain the discontinuous nature of this transition.

1. Introduction

Understanding the stability of dynamical systems is a fundamental question in various fields of science, ranging from ecology [1, 2] and economics [3, 4] to neuroscience [5] and chemistry [6, 7]. In many cases, the stability analysis of a dynamical system can be reduced to a spectral problem involving a matrix, as discussed in [8, 9]. Therefore, there has been significant interest in understanding how the statistical properties of matrix elements impact the spectral properties of the matrix, which in turn can shed light on the stability of the underlying dynamical system.

As early as the 1970s, using random matrices May has studied, for instance, the stability of fully connected ecosystems [10]. Although this fueled significant interest [11], it is only recently that the influence of sparse network structure on dynamical stability has been studied. Indeed, following pioneering work on the spectra of symmetric Erdős–Rényi graphs [12–15], recent papers studied the spectra of random, directed graphs [16–24] and the spectra of random graphs with predator–prey, mutualistic, or competitive interactions [25].

A surprising finding of these more recent works is that the spectra of sparse random graphs are strongly affected by the sign patterns of their matrix entries, i.e. whether $\mathrm{sign}(A_{ij}A_{ji}) = 0$ (unidirectional interactions), $\mathrm{sign}(A_{ij}A_{ji}) = -1$ (sign-antisymmetric interactions), or $\mathrm{sign}(A_{ij}A_{ji}) = 1$ (sign-symmetric interactions). Notably, the spectra of (infinitely large) sparse random graphs are confined to a region in the complex plane with bounded real part if $\mathrm{sign}(A_{ij}A_{ji}) \in \{0, -1\}$ for all pairs i, j of nodes [21, 25], whereas the

spectra of (infinitely large) sparse random graphs encompass the full real axis if there exists a finite proportion of links with $\text{sign}(A_{ij}A_{ji}) = 1$ [25].

In the present paper, we provide a simple, sufficient criterion for the finiteness of the real part of the leading eigenvalue, which is the eigenvalue with the largest real part, of an infinitely large, sparse, random matrix. To this aim, we rely on the concept of *sign stability*.

Sign stability appeared first in studies on qualitative economics [3, 4] in the 1960s when economists were studying the impact of qualitative properties of interaction matrices on the stability of economic systems, such as, the sign of the elements in the interaction matrices. The importance of sign stability was soon realised for ecology [26–30] and later it was also considered in chemistry [31]. A matrix $\mathbf{M}$ is sign stable if any matrix whose entries have the same signs as the corresponding entries of $\mathbf{M}$ is also stable, i.e. its leading eigenvalue is negative. In order for a matrix to be sign stable, it must satisfy specific constraints on its topology and sign pattern [3, 32]. Interestingly, tree graphs admit sign stable structures, for instance, directed tree graphs and antagonistic tree graphs are sign stable. On the other hand, in general, if cycles are present the sign stability property may be lost.

As sparse random graphs, e.g. sparse Erdős–Rényi graphs, contain cycles, they are not sign stable. However, Erdős–Rényi graphs are locally tree-like [33–35], and as tree graphs admit sign stable structures, we say that Erdős–Rényi graphs are *locally sign stable* if the signs of their interaction patterns correspond those of sign stable trees. A formal definition of local sign stability will be given in section 4 and will apply to a broader class of sparse random graphs. We then propose a stronger version of local sign stability, called in the following *strong local sign stability*, as sufficient condition for the finiteness of the real part of the leading eigenvalue. Hence, we argue that strong local sign stability allows us to predict the stability of large, sparse network structures and extends sign stability to sparse random graphs.

One important aspect of sign stability, which also applies under mild conditions, as discussed later, to (strong) local sign stability, is that it refers to all matrices with the same topology and sign pattern, independently from the absolute value of their nonzero elements. Sign stability is therefore a particularly robust type of stability, as it characterises an infinitely large set of matrices. This aspect is particularly relevant in ecological applications for at least two reasons. First, most of the time, as discussed in the following section, to determine whether $\mathbf{M}$ is stable we need to determine its leading eigenvalue, which requires knowledge of the matrix entries M_{ij}. Unfortunately, in applications it is often the case that only partial information about the matrix $\mathbf{M}$ is available. For example, in the context of ecology, it is relatively easy to determine both the foodweb of the trophic interactions between species, i.e. whether $M_{ij} = 0$ or $M_{ij} \neq 0$, and the type of the interactions, inter alia, predator–prey (corresponding to sign-antisymmetric), mutualistic or competitive (corresponding to sign symmetric, respectively positive or negative) interactions. On the other hand, it is significantly more difficult to determine the strengths $|M_{ij}|$ of the trophic interactions between species [2, 36]. This raises the question whether stability can be determined from the sign pattern of the entries of the matrix $\mathbf{M}$. Second, different kinds of ecosystem stability (linear stability, structural stability, feasibility) can be studied by looking at the properties of different matrices obtained from the matrix $\mathbf{A}$ of inter-species interactions without sign or topological alterations. In these cases, as explained in more details in the following section, if the topological properties and the sign pattern of the interaction network grant its strong local sign stability, the ecosystem can be declared at once feasible and stable, both with respect to small fluctuations and small changes in the external conditions.

A second interesting problem for sparse random graphs that we address is whether the leading eigenvalue is real-valued or whether it has a nonzero imaginary part. As it will be recalled, the presence of pairs of conjugate complex leading eigenvalues has important consequences on the dynamical behaviour of the models associated as it gives rise to oscillatory dynamics in the vicinity of the fixed point with frequency of oscillations inversely proportional to the absolute value of the imaginary part of the leading eigenvalue. This aspect is especially relevant for strongly locally sign stable random graphs, as their leading eigenvalue is finite. In particular for these cases, we will discuss how depending on the choice of model's parameter both situations can arise and we will describe the transition between the two corresponding dynamical phases.

The paper is structured as follows: we first review in section 2 the problem of stability in ecology, including a general discussion on the dependence of stability on the system size, and we specify the random matrix models that we study in this paper. In section 3, we review the properties of sign stability with particular attention to its occurrence in tree graphs, before presenting the main results of this paper in the sections 4 and 5. In section 4, we present the paper's main claim: we identify strong local sign stability as an important feature for the spectra of sparse random matrices and the stability of complex systems. We also present several numerical results through direct diagonalisation of the models of sparse random matrices, as defined in section 2. In particular, we test the strong local sign stability criterion by showing that if its conditions hold the leading eigenvalue remains finite. We also show how significant the main conditions are by giving examples of ensembles that violate one of the conditions and show divergence of the leading

eigenvalue. In section 5, we determine the imaginary part of the leading eigenvalue for several type of sparse, random graphs, and in particular we identify a transition from a regime where the leading eigenvalue is real to a regime where the leading eigenvalue come in a pair of complex eigenvalues. We end the paper with a discussion in section 6, and a few Appendices with technical details.

2. Stability in ecology and model setup

In this section, we introduce the model setup of this paper. In sections 2.1 and 2.2, we review the relation between, on one hand, the spectral properties of matrices and, on the other hand, the stability of linear dynamical systems and (nonlinear) ecosystems, respectively. The reader not needing the basic mathematical background or not interested in the ecological applications can skip these two sections. In section 2.3, we review the concepts of absolute and size-dependent stability, which play an important role in this paper. Lastly, in section 2.4, we define the random matrix models that we study in this paper, and in particular in section 2.4.3, we discuss the canonical model parameters that we use.

2.1. Absolute stability and size-dependent stability in linear dynamical systems

Let $\vec{x}(t) \in \mathbb{R}^N$, with $t \geqslant 0$ a time index, denote the evolution in time of the state of a system consisting of N components. The simplest model for a dynamical system of N interacting components is given by a linear differential equation of the form

$$\frac{\mathrm{d}\vec{x}}{\mathrm{d}t} = \mathbf{M}\vec{x}, \tag{1}$$

where $\mathbf{M} \in \mathbb{R}^{N\times N}$ is an arbitrary matrix.

The asymptotic state $\vec{x}_\infty = \lim_{t\to\infty} \|\vec{x}(t)\|$ is determined by the eigenvalues $\lambda_i(\mathbf{M})$ of the matrix $\mathbf{M}$. If all the $\lambda_i(\mathbf{M})$ have negative real parts, then $\vec{x}_\infty = 0$ [8], and we say that the matrix $\mathbf{M}$ is *stable*. On the other hand, if there exists at least one eigenvalue with a positive real part, then $\vec{x}_\infty$ does not exist, as the norm of $\|\vec{x}(t)\|$ diverges for large t, and we say that $\mathbf{M}$ is *unstable*. If we order the eigenvalues such that $\Re[\lambda_1] \geqslant \Re[\lambda_2] \geqslant \ldots \geqslant \Re[\lambda_N]$, where $\Re(\cdot)$ denotes the real part of a complex number, then $\mathbf{M}$ is stable if

$$\Re[\lambda_1] < 0. \tag{2}$$

In the intermediate regime for which

$$\Re[\lambda_1] = 0, \tag{3}$$

we say that the matrix is *marginally stable*. Note that for marginally stable systems $\|\vec{x}(t)\|$ may still diverge as a function of t if the matrix $\mathbf{M}$ has degenerate eigenvalues [37, 38].

Additionally, the transient dynamical behaviour after external perturbations is revealed by the imaginary part of the leading eigenvalue $\lambda_1(\mathbf{M})$, which we denote by $\Im[\lambda_1(\mathbf{M})]$. If $\Im[\lambda_1(\mathbf{M})] = 0$, then the transient is nonoscillatory, whereas a nonzero imaginary part implies oscillatory behaviour of $\vec{x}(t)$ in the vicinity of the origin. The absolute value $|\Im[\lambda_1(\mathbf{M})]|$ determines the frequency of oscillations of the slowest mode if the system is stable, and of the fastest unstable mode if the system is unstable.

Since in this paper we consider large complex systems, following [25], we introduce here two variants of linear stability in the limit of large N. Consider a sequence of matrices $\mathbf{M}_N$ growing in size $N \in \mathbb{N}$. In this case, we can distinguish two classes of matrix sequences, viz., those for which the real part of the leading eigenvalue converges to a finite value, i.e.

$$\lim_{N\to\infty} \Re\left[\lambda_1\left(\mathbf{M}_N\right)\right] \in \mathbb{R}, \tag{4}$$

and those for which

$$\lim_{N\to\infty} \Re\left[\lambda_1\left(\mathbf{M}_N\right)\right] = +\infty. \tag{5}$$

Take as an example of the latter the nondirected star graph $(\mathbf{M}_N)_{ij} = \delta_{i,1}(1-\delta_{j,1}) + \delta_{j,1}(1-\delta_{i,1})$ (with $\lambda_1 = \sqrt{N-1}$, as text book calculation shows [39]) and as an example of the former, the directed star graph $(\mathbf{M}_N)_{ij} = \delta_{i,1}(1-\delta_{j,1})$ (with $\lambda_1 = 0$, which is a simple linear algebra problem), where $\delta_{a,b}$ is the Kronecker delta function. In the former case, there exists a finite $d > 0$ such that

$$\lim_{N\to\infty} \Re\left[\lambda_1\left(\mathbf{M}_N - d\mathbf{1}_N\right)\right] < 0, \tag{6}$$

where $\mathbf{1}_N$ stands for the identity matrix of size $N \times N$, and hence the sequence $\mathbf{M}_N - d\mathbf{1}_N$ is characterised by linear *absolute stability*. In the latter case, any constant shift d renders the ensemble stable up to a certain size $\overline{N}$, such that

$$\Re\left[\lambda_1\left(\mathbf{M}_N - d\mathbf{1}_N\right)\right] < 0, \tag{7}$$

for $N < \overline{N}$, while

$$\Re\left[\lambda_1\left(\mathbf{M}_N - d\mathbf{1}_N\right)\right] > 0, \tag{8}$$

for $N > \overline{N}$, and we speak of *size-dependent stability* of linear systems.

Although linear systems simplify significantly the dynamics of complex systems, they can be insightful for the study of complex systems, such as, ecological systems [11], neural networks [40, 41], chemical interaction networks [42], and economic models [43], whenever the interest is to understand the transient dynamics of systems in the vicinity of a stable fixed point by linearising the system of dynamical equations around the fixed point. We discuss the connection to more general nonlinear dynamics in more detail in the following section, where other types of stability properties for dynamical systems are reviewed on an example of an ecological model and we will generalise absolute stability and size-dependent stability to those cases.

2.2. Stability in ecology

The possibility to predict and control the fate of ecosystems is of immediate concern for our lives, which strongly depend upon them. Therefore the concept of their stability in theoretical ecology has been investigated for decades leading to the classification of different types of stability of potential practical relevance.

We give a brief overview of the different notions of stability studied in the literature. Famously modelled by dynamical systems, ranging from simple one- or two-species population evolution [44, 45] to more recent studies about multi-species interactions [46], ecosystem's stability with respect to small perturbations around putative fixed points has been investigated at length with *linear stability* analyses, [10, 11], accompanied by considerations on their *global* or *local stability*. These approaches assume the existence of at least one equilibrium of ecological relevance, i.e. with nonnegative species' abundances. However it has been pointed out that the conditions for the existence of ecologically meaningful equilibria, called *feasibility*, are far from trivial [47, 48]. Note that in feasible equilibria several species of the original pool can be extinct, and therefore do not enter in the final composition of the ecosystem. Yet, conditions for its *(un-)invadability*, corresponding with linear stability with respect to potential immigration of species, must be explicitly looked at. A different kind of stability is represented by *structural stability*, which refers to the sensitivity of (feasible and linearly stable) equilibria (and of their stability and invadability) to changes in the ecological parameters. The present paper discusses in the same general context feasibility, structural and linear stability of model of ecosystems defined by several types of (sparse) interaction graphs.

The well-known complexity-stability trade-off in models of ecological systems generally affects their feasibility [47–50], linear stability [10, 11, 51, 52] and structural stability [47, 53–57]. Specifically, many models of ecosystems assembled from a pool of S interacting species show a dependence of their stability properties on S. We will refer in short to this situation by calling it *size-dependent stability*. Conversely, we define *absolute stability* the stability property of a system if it is not affected by its system size. A formal definition of size-dependent stability in linear systems can be found in the previous section and its discussion in the general case is in section 2.3. Note that in many cases absolutely stable models can be trivially constructed from models with size-dependent stability by simply rescaling the inter-species interactions by S. However, in absence of direct biological evidences of very weak inter-species interactions, such rescaling can appear unnatural and forced. Therefore in the following we will call absolutely stable only those models for which stationary points of the dynamics can be made available and can be stabilised without rescaling the interactions by the system size.

The natural consequence of size-dependent stability is to severely constraint the possibility for these models to account for the emergence of a large biodiversity. We will discuss how ecosystems whose interactions are structured according to sparse, locally tree-like, graphs, in some special cases, can benefit from absolute stability. Such property will affect for different reasons all the different kinds of stability and feasibility, previously reviewed, allowing rich biodiversity to emerge.

To illustrate the mathematical implications of the different concepts of stability and the ways to address questions about them, we refer to a generalised Lotka–Volterra model where the ith species' abundance $N_i \in \mathbb{R}^+$, with $i \in \{1, 2, \ldots, S\}$, obeys the following dynamical equation

$$\frac{dN_i}{dt} = N_i \left[\left(r_i - \frac{N_i}{K_i} \right) - \sum_{j=1;j\neq i}^{S} \alpha_{ij} N_j \right] + \zeta = N_i f_i \left(\{N_j\} \right) + \zeta, \tag{9}$$

where the $\{\alpha_{ij}\}$ are the entries of the *interaction matrix* **A** and where ζ is the immigration rate (to be sent to zero before extracting the results, but useful to avoid considering ecosystems with trivial extinctions, and therefore to grant uninvadability). The other parameters of the model, appearing in the first self-regulation term on the right hand side, are the growth rates in isolation r_i and the carrying capacities K_i/r_i. Depending on the choice of the graph structure, determined by the nonzero α_{ij} and of their sign and strength, different type of ecological models can be obtained and studied, from unstructured ecosystems to hierarchical food-webs, from predator–prey (sign-antisymmetric) types of interactions to mutualistic or competitive ones.

In this family of models, feasibility requires the existence of fixed points of the dynamics, therefore the existence of at least one non trivial meaningful solution $\vec{N}^*$, with elements $\{N_i^*\}$, to the set of equations $f_i(\{N_j\}) = -\lim_{\zeta\to 0} \zeta/N_i$. All extinct species i will have $N_i^* = 0$ and $f_i(\{N_j^*\}) < 0$, while surviving ones will be characterised by $N_i^* \neq 0$ and $f_i(\{N_j^*\}) = 0$, therefore

$$r_i = \frac{N_i^*}{K_i} + \sum_{j=1;j\neq i}^{S} \alpha_{ij} N_j^* \ . \tag{10}$$

The existence of a solution to the last equation is granted by the invertibility of the matrix **B** with elements

$$B_{ij} = \frac{\delta_{ij}}{K_i} + \alpha_{ij} \tag{11}$$

restricted to the S^* surviving species:

$$\vec{N}^* = \mathbf{B}^{-1} \vec{r} \, . \tag{12}$$

For **B** to be invertible, it is needed that none of its eigenvalue is null or, alternatively, that, in the infinitely large S limit, the continuous part of the spectrum does not include the origin of the complex plane and none of the isolated eigenvalues is null.

Feasibility also requires that all elements in $\vec{N}^*$ are non negative. Explicit characterisation of the probability to observe a feasible equilibrium are determined for ecosystems on dense unstructured graphs [48], some special ecologically inspired structure of the graph [54, 58], and can be studied numerically in some more contexts, but no result is known in general. Naturally, the requirement of having nonnegative abundances is more stringent than the condition for the existence of a solution to equation (10), yet in the case previously studied the failing of the first condition closely anticipate the breaking of the second [48]. Following this observation and in absence of a general rule able to asses full-fledged feasibility, we will consider the condition for the existence of a non trivial $\vec{N}^*$ as a good proxy for feasibility.

Interestingly, the matrix **B** is also directly relevant for structural stability, defined as the stability of the abundances of surviving species, $\vec{N}^*$, to small perturbations of the ecological parameters. In fact, as we show in appendix A, the susceptibility of N_i^* to little variations ξ_i, η_i and ϵ_{ij} of the three ecological parameters r_i, K_i and α_{ij}, respectively, is directly related to the inverse of **B**:

$$r_i \to r_i + \xi_i \implies \frac{\partial N_i^*}{\partial \xi_j} = \left(\mathbf{B}^{-1} \right)_{ij} , \tag{13}$$

$$K_i \to K_i + \eta_i \implies \left. \frac{\partial N_i^*}{\partial \eta_k} \right|_{\vec{\eta}=0} = \left(\mathbf{B}^{-1} \right)_{ik} \frac{N_k^*}{K_k^2} , \tag{14}$$

$$\alpha_{ij} \to \alpha_{ij} + \epsilon_{ij} \implies \left. \frac{\partial N_i^*}{\partial \epsilon_{k\ell}} \right|_{\epsilon=0} = - \left(\mathbf{B}^{-1} \right)_{ik} N_\ell^* \, . \tag{15}$$

Again, in all the three cases above, a singular behaviour emerges if the spectrum of **B** contains the origin of the complex plane hinting to a large susceptibility of the solution of $\vec{N}^*$ to ecological parameters.

Finally, the classical information on linear stability (stability with respect to dynamical fluctuations as induced by demographic noise, for instance), or Lyapunov stability concerning the domains of attraction of

fixed point of the dynamics, is obtained by linearising the system of dynamical equations around the fixed point $\vec{N}^*$ hence therein evaluating the *Jacobian* **J**, *a.k.a.* the *community matrix*, with elements

$$J_{ij} = \left.\frac{\partial\left[N_i f_i\left(\{N_j\}\right)\right]}{\partial N_j}\right|_{\{N_j^*\}} = \delta_{ij} f_i\left(\{N_j^*\}\right) + N_i^* \left.\frac{\partial f_i\left(\{N_j\}\right)}{\partial N_j}\right|_{\{N_j^*\}} . \tag{16}$$

Note that contributions to the Jacobian coming from extinct species is diagonal and negative. The non trivial part comes from the S^* surviving species and it gives rise to the $S^* \times S^*$ matrix

$$J_{ij}^* = -N_i^* B_{ij} , \tag{17}$$

with a non trivial stripy structure where the elements in each row are all rescaled by the same factor N_i^*. As discussed in the section about linear dynamical systems, linear stability requires that the real part of the leading eigenvalue $\lambda_1(\mathbf{J})$ is negative, and a nonzero imaginary part gives rise to oscillatory dynamics in the vicinity of the fixed point with frequency of oscillations inversely proportional to $|\Im[\lambda_1(\mathbf{J})]|$.

The generalised Lotka–Volterra model discussed in this section provides an example of the structure of the matrices of interest when focusing on different facets of the stability of ecological systems. In these structures the interaction matrix **A** always plays an important role on the elements outside the diagonal, while the self regulation mechanism represented by the carrying capacities contributes to the non trivial diagonal. Moreover, in the Jacobian, each row is multiplied by the abundance of the corresponding species at the fixed point. Note that different examples of single species self-regulation mechanisms contained in the definition of f_i, such as those including the so called *Allee effect* [59] for instance, can lead to less straightforward connections between feasibility, structural and linear stability.

A nowadays widespread approach to model ecosystems with large number of species is to account for the large variety of self-regulation and interaction mechanisms by introducing random parameters, so that the matrices **A**, **B**, **J** may be represented by random matrices [10, 11, 46, 60]. In the simple generalised Lotka–Volterra model considered above, this choice would require to introduce at least one probability distribution $p(\alpha)$ for the amplitudes of inter-species interactions α_{ij}. When referring specifically to feasibility or structural stability determined by **B**, the simplest setting would imply assuming uniform growth rates across different species and unitary carrying capacities so that $\mathbf{B}_{\rm Id} = \mathbf{A} + \mathbf{1}$. However, more generally it can be important to include in **B** the contribution of non trivial diagonal terms of a diagonal matrix **D**, which are extracted from a second distribution $p_D(d)$ to describe the variability of carrying capacities $\mathbf{B} = \mathbf{A} + \mathbf{D}$. Recall that the important stability trait of **B** or $\mathbf{B}_{\rm Id}$ is whether the spectrum contains or not the origin, which is answered by checking that the smallest real eigenvalue is positive. Under this perspective it is completely equivalent to check whether the largest real eigenvalue of $-\mathbf{B}$ or $-\mathbf{B}_{\rm Id}$, or equivalently (as long as the spectra of **A** is symmetric around the origin) of $\mathbf{A} - \mathbf{1}$ or of $\mathbf{A} - \mathbf{D}$, is negative. When focusing on **J**, instead, the variability of the stationary abundances N_i^* becomes a more relevant factor in the structure of the matrix. For simplicity, the carrying capacities are then set to the unity, $p_D(d)$ represents the distribution of the abundances, placed on the elements of a diagonal matrix **D**, and we look at $\mathbf{J} = -\mathbf{D}\mathbf{B}_{\rm Id}$, or equivalently at $\mathbf{J} = \mathbf{D}(\mathbf{A} - \mathbf{1})$, checking also in this case that the real part of its leading eigenvalue is negative.

Other key ingredients for model selection are the choice of the sign of interactions α_{ij} and α_{ji} [25, 46, 61] and the graph structure of inter-species interactions [25, 62]. The first aspect is related to which type of ecological behaviour determines the inter-species interactions: mutualistic (both positive), competitive (both negative), or predator–prey (of opposite sign). The first two cases will be also called sign-symmetric and the last sign-antisymmetric. The interaction graph structure that can be considered spans from fully connected graphs to several types of sparse graphs. In this work we focus on the influence of short and long cycles on sparse graphs, therefore we will discuss and compare the results obtained on tree graphs (no cycles), Erdős–Rényi graphs (typical cycles with a length of the order $O(\log(S^*))$, and only a finite number of cycles of fixed length [63]), and pure Husimi trees (cycles of fixed, short, length).

All the ecologically motivated characteristics of the random matrices $\mathbf{B}_{\rm Id}$, **B** and **J** highlighted and discussed in this section will be encoded in the different types of random matrix models introduced in the next section. In that context the ecological notation is abandoned in favour of a more general random matrix notation where N is the size of the matrix instead of S or S^*, and a random diagonal matrix called **D** can either represent the diagonal matrix of inverse carrying capacities, or contain the elements of the vector of abundances $\vec{N}^*$.

2.3. Absolute stability and size-dependent stability for interaction-like and Jacobian-like ensembles

For all the ensembles of random matrices introduced in the previous section, and defined more generally in the next section, we are interested in behaviour of their spectra when the matrix size is large, i.e. $N \gg 1$. The

stability of the corresponding dynamical system is assured if the spectrum of the associated interaction-like matrix does not include the origin of the complex plane and if the spectrum of the corresponding Jacobian-like matrix has leading eigenvalue with negative real part.

As discussed in the previous sections, we distinguish between models whose stability properties are not affected by their system size N, which we call *absolutely stable* models, and models whose stability is lost for N larger than a finite size $\overline{N}$, and hence their stability is *size-dependent*.

Absolute stability, in terms of feasibility, linear, and structural stability, is granted if the real part of all eigenvalues of the corresponding relevant matrix is negative for all N, as discussed in section 2.2. In other words, we require that $\Re[\lambda_i] < 0, \forall i \in \{1, 2, \ldots, N\}$ and $\forall N \in \mathbb{N}$. Therefore, a necessary condition for absolute stability is that the spectra have a *real part bounded from above* in the large size limit, which implies that $\Re[\lambda_i] < a, \forall i \in \{1, 2, \ldots, N\}$ and $\forall N$, where a is a finite constant. In such settings, absolute stability is obtained whenever, for all N, the matrix is equipped with a diagonal that has elements that are smaller than some finite $-d < 0$, such that all eigenvalues have negative real part.

Previous works [11, 61, 64] have shown that the stability of densely connected models does not depend on their sign pattern. Hence, dense matrices are either size-dependent, or become absolutely stable if their matrix entries are properly rescaled by N. Instead, we focus in this paper on sparsely connected models for which, interestingly, the sign pattern of interactions determines whether the matrix is absolutely stable or exhibits size-dependent stability [25]. Indeed, as we are going to discuss in detail in the next sections, for large, sparse, random matrices the existence of a finite upper bound for the real part of all eigenvalues may arise in specific settings without the need of any *ad-hoc* global rescaling by system size, contrarily to the case of dense models.

2.4. Random matrix models built from graphs

We define the random matrix models that we study in this paper. All the random matrix models are built from underlying graphs by using the weights of the edges as matrix entries. In particular entries opposite to the diagonal represent the weights of edges pointing to opposite directions. The matrix entry is zero if the corresponding directed edge is absent. An edge is called nondirected if the two corresponding entries of the matrix are both nonzero.

2.4.1. The model structure

We distinguish two type of random matrices defined on sparse random graphs, namely, *interaction-like* matrices **B**, and *Jacobian-like* matrices **J**. Both matrices **B** and **J** are obtained from an *interaction* matrix **A** that is the adjacency matrix of a weighted graph, and which specifies the network of interactions between the system constituents.

Interaction-like matrices are the sum of the interaction matrix **A** and a diagonal matrix **D**, i.e.

$$\mathbf{B} := \mathbf{A} - \mathbf{D}, \tag{18}$$

where the entries $D_i \geqslant 0$ are independent and identically distributed random variables drawn from a distribution $p_D(d)$ with $d \in \mathbb{R}^+$, and the interaction matrix **A** will be defined in the next subsection. In the special case of $D_i = 1$, for all i, we get what we call the *shifted interaction* matrix

$$\mathbf{B}_{\mathrm{Id}} := \mathbf{A} - \mathbf{1}, \tag{19}$$

where **1** is the identity matrix.

Instead, *Jacobian-like* matrices **J** are defined as the product of $\mathbf{B}_{\mathrm{Id}}$ with **D**, viz.,

$$\mathbf{J} := \mathbf{D}\mathbf{B}_{\mathrm{Id}}, \tag{20}$$

where the entries $D_i \geqslant 0$ are as before independent and identically distributed random variables drawn from a distribution $p_D(d)$ with $d \in \mathbb{R}^+$ and finite second moment.

*2.4.2. The interaction matrix **A***

The random matrices **A** have elements

$$A_{ij} := C_{ij}\alpha_{ij}, \tag{21}$$

where $C_{ij} \in \{0, 1\}$ are the entries of the adjacency matrix of a nonweighted, nondirected, random graph, and the $\alpha_{ij} \in \mathbb{R}$ are the weights of the edges of the graph, which represent the strengths of the interactions.

The weights α_{ij} and α_{ji} are pairs of random variables extracted from a probability distribution $p_\alpha(u,l)$ that is symmetric under the exchange of its arguments, viz.,

$$p_\alpha(u,l) := p(|u|)\,p(|l|)\,\vec{\theta}(u)\,\mathbf{\Pi}\left(\pi^{\mathrm{S}},\pi^{\mathrm{O}}\right)\,\vec{\theta}^{\,T}(l)\,, \tag{22}$$

where $\vec{\theta}(x) = \{\vartheta(x),\vartheta(-x)\}$, $\vartheta(x)$ is the Heaviside function,

$$\mathbf{\Pi}\left(\pi^{\mathrm{S}},\pi^{\mathrm{O}}\right) := \begin{pmatrix} \pi^{\mathrm{S}}\left(1-\pi^{\mathrm{O}}\right) & 0.5\pi^{\mathrm{O}} \\ 0.5\pi^{\mathrm{O}} & \left(1-\pi^{\mathrm{S}}\right)\left(1-\pi^{\mathrm{O}}\right) \end{pmatrix}, \tag{23}$$

and $p(x)$ is a probability distribution supported on $\mathbb{R}^+$ and with finite second moment; notice that we are particularly interested in models with unbounded support as their norm diverges in the infinite size limit, which is important for the findings in this paper. The constants π^{O} and π^{S} determine the (anti)correlation between the sign of α_{ij} and the sign of α_{ji} (their absolute values are uncorrelated). For $\pi^{\mathrm{O}} = 1$ elements opposite to the main diagonal of $\mathbf{A}$ have opposite signs, i.e. $\alpha_{ij}\alpha_{ji} < 0$, which we call *sign-antisymmetric* interactions. In this case, we speak of *antagonistic* model. If $\pi^{\mathrm{O}} = 0$, then elements opposite to the main diagonal have the same sign, i.e. $\alpha_{ij}\alpha_{ji} > 0$, and we speak of *sign-symmetric* interactions. The elements are positive if $\pi^{\mathrm{S}} = 1$ and negative if $\pi^{\mathrm{S}} = 0$, sometimes referred to as mutualistic and competitive interactions, respectively [61]. For intermediate values of $\pi^{\mathrm{O}} \in (0,1)$, we speak of a *mixture* models, as it contains a mixture of sign-antisymmetric and sign-symmetric interactions.

For the adjacency matrix C_{ij} we focus in this paper on two models. One is a random graph model that is locally tree-like, i.e. it has a small number of cycles of small length. The second model is deterministic and has many cycles of small length. In this way, we will be able to address the effect of cycles on our results. The models considered are:

- *Erdős–Rényi graphs*: There are two closely related variants of the Erdős–Rényi (ER) random graph model [65, 66]. In the first model, a graph is chosen uniformly at random from the collection of all graphs which have N nodes and M edges. In the second model, the number of nodes N is fixed and each edge connecting two of them exists with a probability q, which is fixed and independent from every other edge. The Erdős–Rényi graphs we use are built according to the second model, that we denote as $G(N,q)$, setting $q = c/(N-1)$ where c is it is the average number of edges on a single node, also called *connectivity* of the node. In the limit $N \to \infty$, with c fixed, Erdős–Rényi graphs are locally tree-like graph in the sense that with probability one the finite neighbourhood of a randomly selected node is a tree, the typical cycles length ℓ grows like $\log N$ [33–35], and they have only a finite number of cycles of fixed length [63]).
- *Husimi trees*: Husimi trees are connected graphs for which no edge lies on more than one cycle [67]. Loosely said, Husimi trees are trees built out of edges and cycles, such as, triangles, quadrilaterals, pentagons, etc. Husimi trees were introduced by Harary and Uhlenbeck [67], who recognised this graph structure in Husimi's virial expansion of the equation of state of a nonideal gas [68], and whose terminology we adapt in this paper. If Husimi trees are built out of one type of cycle, then one speaks of pure Husimi trees, as in panel (c) of figure 1, while otherwise they are mixed Husimi trees. If the cycles are triangles, then one speaks of a Husimi cactus. If the tree structure is regular with coordination number c, a pure Husimi tree with cycles of length ℓ can be defined by using the notation (c,ℓ)-pure Husimi tree. For instance, a $(c,1)$-pure Husimi tree is a Cayley tree or a Bethe lattice. Note that (c,ℓ)-pure Husimi trees have a number of cycles of fixed length ℓ growing linearly with the system size.

As a recap, the models studied across this work can be identified from the matrix structure (interaction-like $\mathbf{B}$, shifted interaction $\mathbf{B}_{\mathrm{Id}}$, Jacobian-like $\mathbf{J}$), the choice of the distributions p and p_D, the interactions sign pattern (antagonistic, mixture), and the graph structure encoded in $\mathbf{C}$ (tree, $G(N,q)$ Erdős–Rényi graphs, (c,ℓ)-pure Husimi tree).

2.4.3. Canonical model parameters

Here we list the parameters that we use in the numerical results shown in the following sections. Any variations on these will be reported in the figures captions.

As anticipated, we deal with three matrix structures, viz., shifted interaction matrices $\mathbf{B}_{\mathrm{Id}} = \mathbf{A} - \mathbf{1}$, interaction-like matrices $\mathbf{B} = \mathbf{A} - \mathbf{D}$ and Jacobian-like matrices $\mathbf{J} = \mathbf{D}\mathbf{B}_{\mathrm{Id}}$. In numerical examples, we need to specify the adjacency matrix $\mathbf{C}$, the distribution p_α of weights $(\alpha_{ij},\alpha_{ji})$, and the distribution p_D of diagonal entries D_i.

We consider two ensembles of adjacency matrices $\mathbf{C}$, viz., sparse, Erdős–Rényi graphs and Husimi trees. Erdős–Rényi graphs are drawn from the $G(N,q)$ model with $q = c/(N-1)$. Since we are interested in sparse graphs, the connectivity is kept fixed at $c = 2$, and thus does not scale with the graph size N. The Husimi trees

that we employ are $(4,4)$-pure Husimi tree, and hence all cycles have length $\ell = 4$, as shown in panel (b) of figure 2 for the case of a Husimi tree dressed with sign-antisymmetric interactions.

For the probability distribution p of the absolute values $|\alpha_{ij}|$ of the off-diagonal matrix entries α_{ij}, which appears in equation (22), we use a truncated Gaussian distribution. In particular, we truncate a Gaussian distribution with mean $\mu_G = 1.0$ and variance $\sigma_G = 0.6$ so that it is supported on the positive part of the real line, viz.,

$$p(x) = \frac{2}{1 + \mathrm{erf}\left(\frac{\mu_G}{\sqrt{2\sigma_G^2}}\right)} \vartheta(x)\, \mathcal{G}_{\mu_G,\sigma_G}(x) \tag{24}$$

where $\mathcal{G}_{\mu_G,\sigma_G}(x)$ is a Gaussian distribution with mean μ_G and variance σ_G, $\mathrm{erf}(x)$ is the error function, and $\vartheta(x)$ is the Heaviside function.

Notice that the first two moments of the truncated Gaussian distribution take the expressions

$$\mu_{TG} := \langle x \rangle_{TG} = \mu_G + \sqrt{\frac{2}{\pi}}\sigma_G \frac{\exp\left(-\frac{\mu_G^2}{\sigma_G^2}\right)}{1 + \mathrm{erf}\left(\frac{\mu_G}{\sqrt{2\sigma_G^2}}\right)} \tag{25}$$

and

$$\langle x^2 \rangle_{TG} = \mu_G^2 + \sigma_G^2 + \sqrt{\frac{2}{\pi}}\mu_G\sigma_G \frac{\exp\left(-\frac{\mu_G^2}{2\sigma_G^2}\right)}{1 + \mathrm{erf}\left(\frac{\mu_G}{\sqrt{2\sigma_G^2}}\right)}\,, \tag{26}$$

where $\langle\cdot\rangle_{TG}$ denotes the average with respect to the truncated Gaussian distribution. From equations (22), (25), and (26), the first two cumulants of the distribution $p_\alpha(u,l)$ of the off-diagonal element pairs follow readily as

$$\mu := \langle u \rangle = \langle l \rangle = 0, \tag{27}$$

$$\sigma^2 := \langle u^2 \rangle = \langle l^2 \rangle = \langle x^2 \rangle_{TG}, \tag{28}$$

and

$$\langle ul \rangle = \left(1 - 2\pi^O\right)\, \mu_{TG}^2 \tag{29}$$

where $\langle\cdot\rangle$ denotes the average with respect to $p_\alpha(u,l)$.

The matrix sign pattern is set by the choices of π^O and π^S as defined in equation (23). In our work we focus on antagonistic models with $\pi^O = 1$ in which the interactions are sign-antisymmetric and mixture models with $\pi^O = 0.9$ and $\pi^S = 0.5$, characterised by a majority of sign-antisymmetric interactions and a smaller portion of sign-symmetric ones.

In numerical examples we are using for p_D a uniform distribution supported on $[d_{\min}, d_{\max}]$, i.e.

$$p_D(d) = \frac{1}{d_{\max} - d_{\min}}\, \vartheta(x - d_{\min})\, \vartheta(d_{\max} - x) \tag{30}$$

where $d_{\min}$ and $d_{\max}$ are, respectively, the minimum and maximum values of the uniform distribution. Notice that

$$d_{\min} = \mu_D - \sigma_D\sqrt{3} \qquad \text{and} \qquad d_{\max} = \mu_D + \sigma_D\sqrt{3}, \tag{31}$$

where μ_D and σ_D are the mean and standard deviation of p_D, respectively.

We choose $\mu_D > 0$ and $\sigma_D < \mu_D/\sqrt{3}$ such that $p_D(d)$ is supported on a subset of the positive real axis and, thereby, all the D_i are positive. More specifically, in section 4 we set $\mu_D = 1$ and $\sigma_D = 0.5$, whereas in section 5 we set $\mu_D = 1$ and σ_D takes values equally spaced between 0 and 0.30.

We diagonalise matrices with linear algebra routines of the Numpy submodule *linalg* of Python3.

3. Sign stable matrices

We review sign stability of matrices $\mathbf{M} \in \mathbb{R}^{N\times N}$, which plays an important role in this paper, as we extend this concept to random graphs in the next section. As anticipated in the Introduction, sign stability refers to all matrices with the same topology and sign pattern, independently from the value of their nonzero elements. Therefore, sign stability was introduced in studies on qualitative economics in the 1960s [3, 4, 30], and found a decade later applications in, among others, qualitative ecology [26–29], and chemistry [31].

We say that a matrix $\mathbf{M}$ is *sign stable* if any matrix $\mathbf{M}'$ with the same sign pattern is stable. Note that sign stability is a stronger condition than stability, as it requires that the real part of the eigenvalues of all matrices $\mathbf{M}'$ in the equivalence class

$$\mathcal{M}(\mathbf{M}) := \left\{ \mathbf{M}' \in \mathbb{R}^{N\times N} : \operatorname{sign}\left(M'_{ij}\right) = \operatorname{sign}\left(M_{ij}\right) \right\} \tag{32}$$

are negative, where $\operatorname{sign}(x) \in \{-, 0, +\}$. Note that matrices $\mathbf{M}'$ in the equivalence class $\mathcal{M}(\mathbf{M})$ can be generated from $\mathbf{M}$ through

$$M'_{ij} = y_{ij} M_{ij}, \tag{33}$$

where $y_{ij} > 0$. Also, note that $\mathcal{M}(\mathbf{M}_1) = \mathcal{M}(\mathbf{M}_2)$, for all $\mathbf{M}_2 \in \mathcal{M}(\mathbf{M}_1)$.

On first sight, sign stability may appear as a too strong condition to be useful. However, as will become soon evident, there exist several, interesting examples of equivalence classes $\mathcal{M}$ that are sign stable. Moreover, antagonistic, sign stable matrices have a tree structure, which will make them important for the spectral theory of random graphs that we discuss in the next section. In what follows we discuss necessary and sufficient conditions for the sign stability of the equivalence class $\mathcal{M}$ generated by the matrix $\mathbf{M}$.

In the case where $M_{ii} < 0$ for all i, sufficient and necessary conditions for sign stability have been derived by Quirk and Ruppert [3]. These are (see theorem 3 in [3]):

$$M_{ij} M_{ji} \leqslant 0, \quad \forall i \neq j, \tag{34}$$

and for all $m \geqslant 3$,

$$M_{i_m i_1} = 0, \quad \forall i_1 \neq i_2 \neq \cdots \neq i_m, \quad \text{such that,} \quad M_{i_1 i_2} M_{i_2 i_3} \ldots M_{i_{m-1} i_m} \neq 0. \tag{35}$$

Condition (34) implies that edges are either directed or nondirected with sign-antisymmetric weights, and condition equation (35) states that there are no directed cycles of length $m \geqslant 3$.

In the case where $M_{ii} \leqslant 0$, the conditions equations (34) and (35) are sufficient and necessary conditions for marginal, sign stability (see lemma 5 in [3]). In [27, 32, 69] the marginal stable case has been studied in more detail, in particular to determine the conditions for which $\lim_{t\to\infty} \|\vec{x}(t)\|$ diverges.

We will not discuss the derivation of the conditions equations (34) and (35), as these can be found in detail in [3, 32]. Nevertheless, we mention three notable examples of sign stable matrices and show that they are sign stable:

- *Nondirected antagonistic tree graphs*: this is a tree graph with sign-antisymmetric edges, i.e. $M_{ij} > 0 \Leftrightarrow M_{ji} < 0$ for all $i \neq j$, as illustrated in panel (a) of figure 1. The condition (34) ensues from the sign-antisymmetric nature of the edges, and the condition (35) from the absence of cycles in a tree graph implies condition. The sign stability of nondirected antagonistic tree graphs follows from the fact that (i) tree graphs with sign-antisymmetric interactions and negative diagonal elements have eigenvalues with negative real part, as we show in appendices B and C; (ii) the sign-antisymmetric nature of the interactions is preserved in the equivalence class $\mathcal{M}$ generated by an antagonistic tree graph. Note that this example will be referred to extensively in the remainder of the paper. Importantly, simply lifting the constraint of sign-antisymmetric edges, as shown in panel (a) of figure 2, will determine also in the case of a tree graph the failing of condition equation (34). The corresponding matrices are not sign stable anymore.
- *Oriented tree graphs*: these are the adjacency matrices of tree graphs with unidirectional edges, as sketched in panel (b) of figure 1. The unidirectionality of the edges implies

$$M_{ij} M_{ji} = 0, \quad \forall i \neq j, \tag{36}$$

and hence equation (34), and the absence of cycles in a tree graph implies condition equation (35). The sign stability of oriented tree graphs follows readily from the following two facts: (i) all eigenvalues of oriented

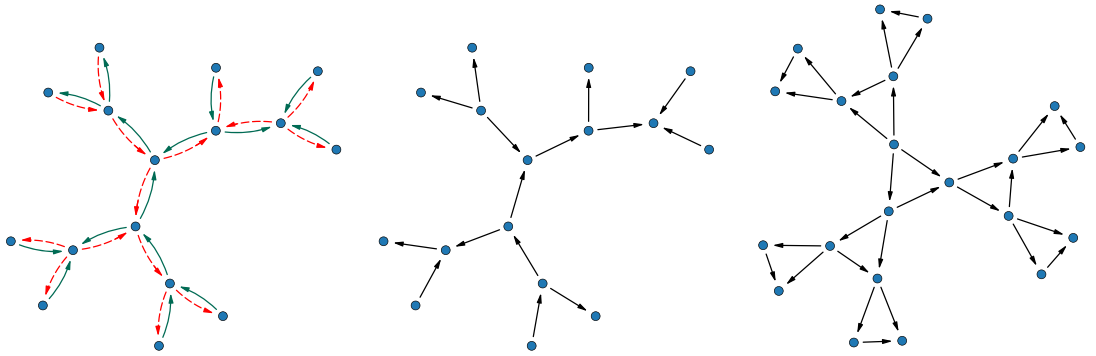

(a) Antagonistic tree (b) Oriented tree (c) Feedforward oriented Husimi tree

Figure 1. Canonical examples of sign stable graphs. The arrows show the orientation of interactions. The colour/style shows the sign of the weights associated with the edges.

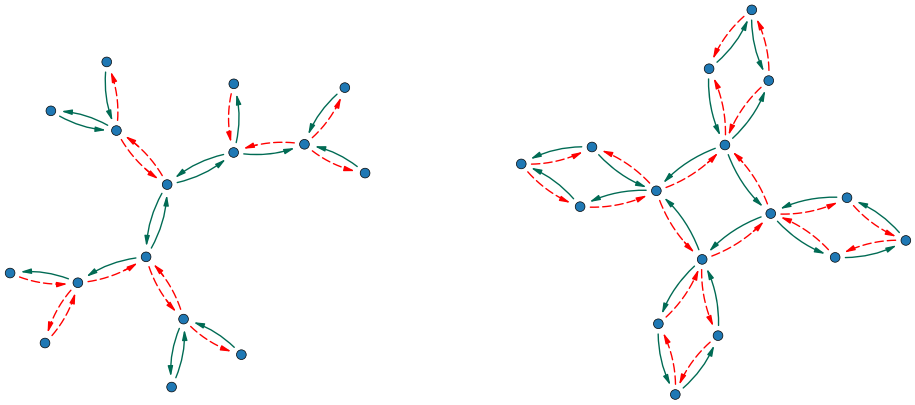

(a) Mixture tree graphs (b) Antagonistic Husimi tree

Figure 2. Examples of graphs that are not sign stable due to the type of interactions (a) or graph topology (b). The arrows show the orientation of interactions. The colour/style shows the sign of the weights associated with the edges.

tree graphs are equal to zero [21, 70], which is a direct consequence of the Coefficients Theorem for Directed Graphs, see appendix D; (ii) the oriented tree property is preserved in the equivalence class $\mathcal{M}$ generated by an oriented tree graph.

- *Husimi trees built out of unidirectional feed-forward cycles*: these are Husimi trees built out of motifs that are feedforward cycles, as illustrated in panel (c) of figure 1. Adjacency matrices of such graphs are sign stable for exactly the same reason as the adjacency matrices of oriented tree graphs: (i) $\lambda_j = 0$ for all values of j, see appendix D; (ii) the orientedness and feedforward structure are preserved in the equivalence class $\mathcal{M}$ generated by Husimi trees built out of unidirectional feed-forward cycles. Note that, if on this graph structure we consider instead antagonistic interactions, as shown in panel (b) of figure 2, the condition equation (35) will not be satisfied anymore as feedback loops are created, and the corresponding ensemble of matrices cannot be said to be sign stable.

Note that not all sign stable matrices are tree graphs or Husimi trees. Let's comment on a couple of simple notable examples to illustrate how general is the concept of sign stability. An upper-diagonal matrix with negative entries on the diagonal is a sign stable matrix on any graph structure, even fully connected, as all eigenvalues correspond to the element on the diagonal. On the other hand, antisymmetric matrices for which the entries satisfy $M_{ij} = -M_{ji}$ and $M_{ii} = 0$, are not sign-(marginally)stable, although having all imaginary eigenvalues, similarly to antagonistic tree graphs with zero diagonal entries (see appendix B). The reason is that, at variance with antagonistic tree graphs with zero diagonal entries, most matrices in the corresponding equivalence class $\mathcal{M}$ of antisymmetric matrices are not marginally stable, because they are not antisymmetric and their eigenvalues can have nonnull (positive and negative) real parts.

A further comment on the extension of sign stable ensembles is that adding negative terms to the diagonal of matrices in a sign stable random matrix ensemble does not affect their stability. This leads to an asymmetry in the spectra of sign stable matrices, as the real part of the eigenvalues is bounded from above, but can extend towards infinity on the negative real axis.

Finally, the two examples of graphs shown in figure 2 refer to ensembles which will not be characterised by sign stability due to the fact that either the condition equation (34) or the condition equation (35), respectively, are not satisfied.

4. Implications of local sign stability on the spectra of random graphs

In this section, we identify a useful criterion, which we call *strong local sign stability*, for the finiteness of the ensemble average of the real part of the leading eigenvalue of infinitely large, sparse, random graphs, i.e. $\lim_{N\to\infty}\langle\Re[\lambda_1]\rangle < \infty$; such random matrix models can be made absolutely stable through a constant shift of the diagonal entries, as we discussed in section 2.3.

To introduce local sign stability and strong local sign stability, we first review the results of [25] on the asymptotic behaviour of the real part of the leading eigenvalue of Erdős–Rényi graphs. This paper shows that the average, real part of the leading eigenvalue of an Erdős–Rényi graphs with sign-antisymmetric weights converges to a finite limit as a function of N. This result came as a surprise as the norm of the associated adjacency matrix diverges in the infinite size limit. Moreover, it is sufficient to decorate the Erdős–Rényi graph with a finite fraction of sign-symmetric weights to have a $\langle\Re[\lambda_1]\rangle$ that diverges as a function of N, as expected for an Erdős–Rényi ensemble with diverging norm.

In what follows, we identify the property underlying the finiteness of the real part of the leading eigenvalue in Erdős–Rényi graphs with sign-antisymmetric weights, and we aim to extend this property so that it can be applied to other random graph ensembles. To understand the distinction between Erdős–Rényi graphs with sign-antisymmetric and sign-symmetric weights, we build on the locally tree-like property of Erdős–Rényi graphs, see e.g. [33–35]. We say that a random graph is locally tree-like if for large enough values of N the finite neighbourhood of a randomly selected node is almost certainly a tree. As discussed in section 3, trees with sign-antisymmetric weights are sign stable, whereas this property does not hold for trees with sign-symmetric weights. However, in general, random graphs have simple cycles and hence, given the condition in equation (35), are not sign stable. As a consequence, we can not rely directly on the concept of sign stability introduced in the previous section to understand the distinction between antagonistic and mixture Erős-Rényi graphs.

This limitation leads us to introduce the weaker condition of local sign stability: *let* $\mathbf{M}_N$ *be a sequence of matrices built from weighted graphs of N nodes. Let* $\mathbf{M}_N^{(i)}(d)$ *be the matrix of the weighted subgraph generated by a uniformly and randomly selected node i and all of its nodes located within a distance d of i. We say that* $\mathbf{M}_N$ *is locally sign stable if for all fixed d, the probability that* $\mathbf{M}_N^{(i)}(d)$ *is sign stable converges to one as a function of N.*

In the above definition we consider a matrix built from the graph as explained in section 2.4. In full generality this definition of local sign stability remains valid for graphs that are not locally tree-like as long as the short cycles satisfy the condition given by equation (35). However, for nondirected graphs local sign stability requires locally tree-likeness, as cycles with nondirected edges cannot satisfy the equation (35).

For nondirected graphs we make a step further and introduce the condition of strong local sign stability: *let* $\mathbf{M}_N$ *be a sequence of matrices locally sign stable. We say that* $\mathbf{M}_N$ *is strongly locally sign stable if in addition the average number of cycles of fixed length does not asymptotically increase with N*, which for nondirected graphs is a more stringent requirement than the locally tree-likeness.

Since (strong) locally sign stable matrices are not sign stable, they can have a leading eigenvalue with a positive real part. Nevertheless, finite neighbourhoods $\mathbf{M}_N^{(i)}(d)$ of large tree-like antagonistic graphs are almost certainly sign stable. Thus, sign stability is broken by either cycles of length $\ln(N)$, which diverge for large enough size N, or by a small number of cycles of finite length. Moreover, if the number of finite cycles is small but still growing with N [63], the leading eigenvalue can also still grow with N. Conversely, here we claim that if the number of finite cycles remains finite, as required by the strong local sign stability condition, the real part of the leading eigenvalue can be positive, but will not grow indefinitely when N increases.

We summarise this implication as follows. Consider a set $\mathscr{M}$ of sequences $\{\mathbf{M}_N\}_{N\in\mathbb{N}}$ of random graph models, as defined in section 2.4. Then,

$$\{\mathbf{M}_N\}_{N\in\mathbb{N}} \text{ is strongly locally sign stable} \Longrightarrow \lim_{N\to\infty}\langle\Re\left[\lambda_1\left(\mathbf{M}_N\right)\right]\rangle < \infty. \tag{37}$$

This implication holds (trivially) if the matrix norm $\|\mathbf{M}_N\|$ is bounded. Indeed, the matrix norm is always larger or equal than the real part of the leading eigenvalue, i.e. $\|\mathbf{M}_N\| \geqslant \Re[\lambda_1(\mathbf{M}_N)]$ [71]. The interesting cases arise when $\lim_{N\to\infty}\|\mathbf{M}_N\| = \infty$, e.g. for the weighted Erdős–Rényi graphs that we consider in this

paper. If the matrix norm diverges with the system size, equation (37) remains valid provided that the elements of the matrix have finite second moment.

Equation (37) characterises a sufficient condition, but strong LSS is not necessary to have finite $\Re[\lambda_1]$. Indeed, for instance, for antisymmetric matrices $\mathbf{M}_N$ it holds that $\Re[\lambda_1] = 0$, as all eigenvalues are immaginary, irrespectively of strong local sign stability. Nevertheless, strong LSS can be used as a condition to predict if the leading eigenvalue will have a finite real part and hence whether the corresponding dynamical system can be made absolutely stable or not. To confirm the validity of this condition we rely on known results from the literature on spectra of graphs and we show new numerical results further corroborating the stated condition.

First, let us consider known results on spectra of random graphs. For weighted random oriented graphs an explicit expression for the leading eigenvalue was derived in [21–23], which shows that the leading eigenvalue of large graphs is a growing function of the branching ratio and of the first or the second moment of the weights. Interestingly, the average number of cycles of finite length ℓ also is a growing function of the branching ratio [21]. Hence, for finite second moment of the distribution of weights, both diverge as soon as the branching ratio diverges with the system size. Therefore, in this example strong local sign stability, granted by a finite number of small cycles, implies that the leading eigenvalue is finite, provided that the distribution of weights has a well defined second moment. Another example of a strongly locally sign stable random graphs are Erdős–Rényi graphs (which have finite number of cycles of fixed length) with sign-antisymmetric weights: [25] shows that the real part of the leading eigenvalue is finite as well in this case. On the other hand, symmetric Erdős–Rényi graphs do not satisfy local sign stability condition equation (34) and their spectra contain the whole real axis in the infinitely large limit, see e.g. [12, 13, 72, 73].

In absence of full proof in the general case, and since examples already present in literature are limited, we now employ new numerical simulations to further verify equation (37) for different types of matrix structure. To illustrate the significance of the condition in equation (37) we also explore two settings in which LSS does not hold and the leading eigenvalue grows with the system size. In particular we break strong LSS and LSS in two different ways by removing one of their two fundamental ingredients at a time: sign-antisymmetric entries and the locally tree-like structure. We compare spectral results for antagonistic (i.e. purely sign-antisymmetric) Erdős–Rényi graphs, which according to our definition are strongly locally sign stable, with two matrix ensembles that are not LSS, namely, mixture Erdős–Rényi graphs (i.e. locally tree-like but with a small fraction of sign-symmetric links) and antagonistic Husimi trees (i.e. keeping the sign-antisymmetric links, while dropping the locally tree-like structure).

Since different stability criteria rely on different type of matrices, we consider three cases, as introduced in section 2, namely, shifted interaction matrices $\mathbf{B}_{\mathrm{Id}}$ in section 4.1, interaction-like matrices $\mathbf{B}$ in section 4.2, and Jacobian-like matrices $\mathbf{J}$ in section 4.3.

4.1. Shifted interaction matrices $\mathbf{B}_{\mathrm{Id}}$

First, we illustrate the implication in equation (37) on shifted interaction matrices, $\mathbf{B}_{\mathrm{Id}} = \mathbf{A} - \mathbf{1}$, as defined in section 2.4. The $\mathbf{B}_{\mathrm{Id}}$ matrices are the simplest class of matrices that we consider, as the diagonal entries are constant, and hence we can focus on the contribution of the off-diagonal matrix entries to the spectrum. Note that this matrix structure was also studied in [25], but here for convenience we present again its results (obtained with a different weights distribution) also in comparison with the spectra of antagonistic Husimi trees that has not been considered before.

Figure 3 plots the average value of the real part of the leading eigenvalue, $\langle \Re[\lambda_1(\mathbf{B}_{\mathrm{Id}})] \rangle$, as a function of N for the three ensembles under study, i.e. antagonistic Erdős–Rényi graphs, mixture Erdős–Rényi graphs, and antagonistic Husimi trees. These results, obtained by numerically diagonalising matrices, confirm that strong local sign stability implies that the leading eigenvalue does not diverge with the system size, while violating one of the conditions of LSS leads to its divergence. In fact, figure 3 shows a qualitative difference in the behaviour of the real part of the leading eigenvalue as a function of the matrix size N: for mixture Erdős–Rényi graphs and antagonistic Husimi trees, $\langle \Re[\lambda_1] \rangle$ increases monotonically as a function of N, while for antagonistic Erdős–Rényi graphs, $\langle \Re[\lambda_1] \rangle$ quickly converges to a finite value. Note that the theoretical results in [25] for the boundary of the spectrum of infinitely large graphs obtained with the cavity method support the numerical observation that in the antagonistic Erdős–Rényi case the leading eigenvalue has a real part which remains finite in the large N limit. Therefore the saturation observed from direct diagonalisation results in the antagonistic case turns out to be representative of the large N behaviour. Based on these grounds, in the following, we will rely on direct diagonalisation results to extrapolate the large N behaviour also for interaction-like and Jacobian-like matrices.

So far, we have considered how strong local sign stability affects the leading eigenvalue of $\mathbf{B}_{\mathrm{Id}}$. Instead now, we investigate the effect of strong local sign stability on the full spectra of matrices $\mathbf{B}_{\mathrm{Id}}$, which are plotted in figure 4.

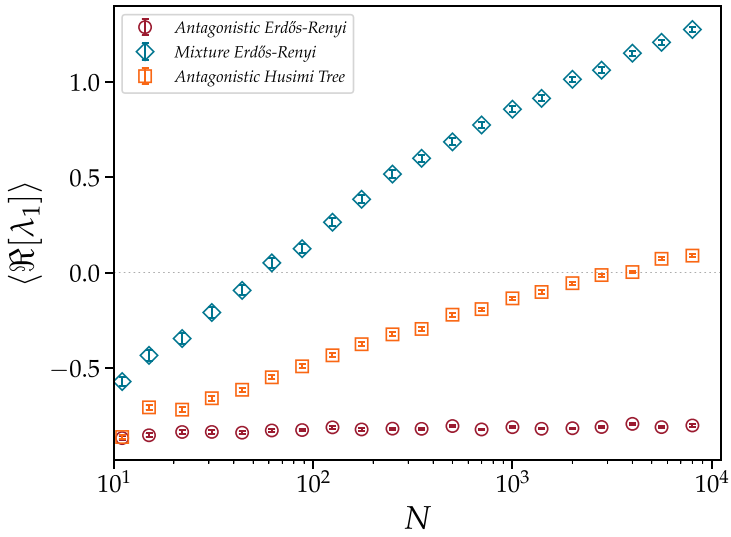

Figure 3. Average real part of the leading eigenvalue, $\langle \Re[\lambda_1] \rangle$, as a function of the matrix size N for shifted interaction matrices $\mathbf{B}_{\mathrm{Id}}$. Results shown are for antagonistic Erdős–Rényi graphs (red circles), mixture Erdős–Rényi graphs (blue diamonds) and antagonistic pure Husimi trees (orange squares). Markers are sample means obtained from numerically diagonalising 300 matrix realisations, and error bars denote the error on the mean. The parameters used for the matrix ensembles are detailed in section 2.4.3.

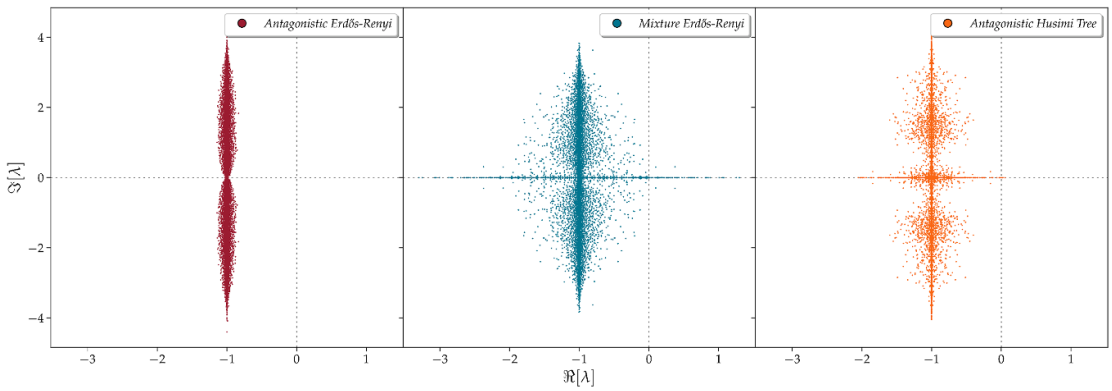

Figure 4. Spectra of shifted interaction matrices $\mathbf{B}_{\mathrm{Id}}$ for antagonistic Erdős–Rényi (red, left), mixture Erdős–Rényi (blue, centre) and antagonistic pure Husimi tree (orange, right). Markers denote the eigenvalues of a single matrix $\mathbf{B}_{\mathrm{Id}}$ of size $N = 8000$. The parameters used are those detailed in section 2.4.3.

Figure 4 shows a qualitative difference between, on one hand, the spectra of antagonistic Erdős–Rényi graphs (red), and on the other hand, the spectra of mixture Erdős–Rényi graphs (blue) and antagonistic Husimi trees (orange). Indeed, in the latter two cases the spectrum develops long tails on the real axis, while in the former case the tails are absent.

Analysing how the spectra evolve as a function of the matrix size N, we have found that the tails on the real axis elongate as the matrix size increases, populating larger and larger portions of the real axis (results not shown), which is in agreement with the results on the divergence of the leading eigenvalue in figure 3. On the other hand, the antagonistic Erdős–Rényi graph has a spectrum that remains confined in a part of the complex plane that has finite width along the real axis, even when the matrix size increases.

Focusing on the imaginary parts of the spectra, we have found that for all three ensembles under study the spectra grow vertically as a function of N, covering an ever larger portion of the imaginary axis. Notice that the latter result is naively expected as the matrix norm diverges as a function of N, and, since $\|\mathbf{M}\| \geqslant |\lambda_i(\mathbf{M})| \ \ \forall i$, there is no simple reason why the eigenvalue should be confined within a finite portion of the complex plane. Hence for the antagonistic, Erdős–Rényi ensemble the divergence of the norm materialises exclusively into the growth of the tails of the spectrum parallel to the imaginary axis.

In light of what we outlined in section 2, the observed qualitative difference in the width of the spectrum on the real axis between ensembles that are strongly locally sign stable and those that are not, indicates that strong local sign stability may be an important characteristic of stability in ecological models. In fact, both

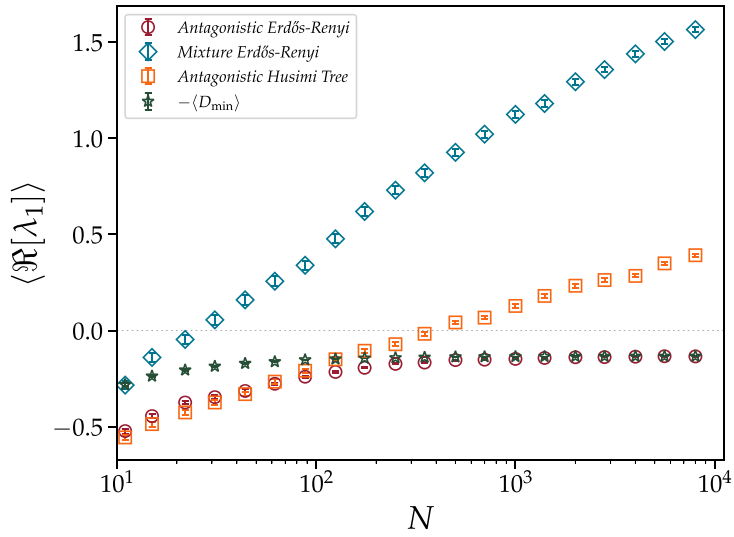

Figure 5. Average real part of the leading eigenvalue, $\langle \Re[\lambda_1] \rangle$, as a function of the matrix size N for interaction-like matrices $\mathbf{B}$. Results shown are for antagonistic Erdős–Rényi graphs (red circles), mixture Erdős–Rényi graphs (blue diamonds) and antagonistic pure Husimi trees (orange squares). The green stars are the averages of the diagonal elements minima. Markers are sample means obtained from numerically diagonalising 300 matrix realisations, and error bars denote the error on the mean. The parameters used for the matrix ensembles are detailed in section 2.4.3.

structural stability and feasibility require that the origin of the complex plane is not part of the spectrum of interaction-like matrices, and therefore, are not compatible with spectra that exhibit tails covering the whole real axis. On the contrary, the spectrum of antagonistic Erdős–Rényi graphs contains a finite portion of the real axis and, therefore, as explained in section 2, the origin of the complex plane can be excluded from the spectrum after a finite shift of the diagonal entries leading to absolutely stable models of ecosystems.

Another interesting feature that we observe in figure 4 is a, so-called, *reentrance effect* in the spectrum of antagonistic Erdős–Rényi graphs. The reentrance effect implies that the width of the spectrum is small for eigenvalues with $\Im[\lambda] \approx 0$. Increasing $\Im[\lambda]$, the width of the spectrum increases until it reaches a maximum at $\Im[\lambda] = \Im[\lambda_1]$, after which the width of the spectrum decreases again to vanish at large values of $\Im[\lambda]$. As a consequence, the leading eigenvalue of antagonistic Erdős–Rényi has typically a finite imaginary part, i.e. $\Im[\lambda_1] \neq 0$, and hence the leading eigenvalue comes in pairs with its complex conjugate. This reentrance effect, which was already observed in [25], will be discussed in-depth in section 5.

4.2. Interaction-like matrices B

In the present section, we confirm the validity of equation (37) also for interaction matrices with fluctuating (negative) diagonal entries, i.e. $\mathbf{B} = \mathbf{A} - \mathbf{D}$, with D_is drawn independently from a distribution p_D supported on a subset of the positive real axis. In particular we choose for simplicity a uniform distribution $p_D(d)$ supported on $[d_{\min}, d_{\max}]$, with $d_{\min} > 0$, even though the main results we obtain for the leading eigenvalue also holds for more general distributions p_D as long as it is supported on $\mathbb{R}^+$.

Figure 5 plots $\langle \Re[\lambda_1(\mathbf{B})] \rangle$ as a function of the matrix size N in the three cases considered before in figure 3, albeit now with a distribution p_D that has a nonzero variance. The results of figure 5 are in correspondence with those of figure 3, further establishing the connection between strong local sign stability and the asymptotic finiteness of the leading eigenvalue. Indeed, for mixture, Erdős–Rényi graphs and antagonistic, Husimi tree graphs the real part of the leading eigenvalue is steadily growing with N, whereas for antagonistic, Erdős–Rényi graphs it converges to a finite value (as a function of N). See more on this comparison in appendix E.

A more detailed look at figure 5 reveals that for small values of $N < 10^2$, the average leading eigenvalue, $\langle \Re[\lambda_1] \rangle$, of the antagonistic Erdős–Rényi graph increases as a function of N, before it eventually saturates at its asymptotic value for $N \gtrsim 10^2$. The transient behaviour of $\langle \Re[\lambda_1(\mathbf{B})] \rangle$ at small values of N is different from the immediate convergence of $\langle \Re[\lambda_1(\mathbf{B})] \rangle$ in figure 3. Moreover, according to figure 5 the asymptotic value is approximately equal to $-d_{\min}$, the largest possible value of the diagonal entries; notice that to consider finite size effects, figure 5 shows in fact $\langle -D_{\min} \rangle$ (green stars), with

$$D_{\min} = \min_{j \in \{1,2,\ldots,N\}} D_j. \tag{38}$$

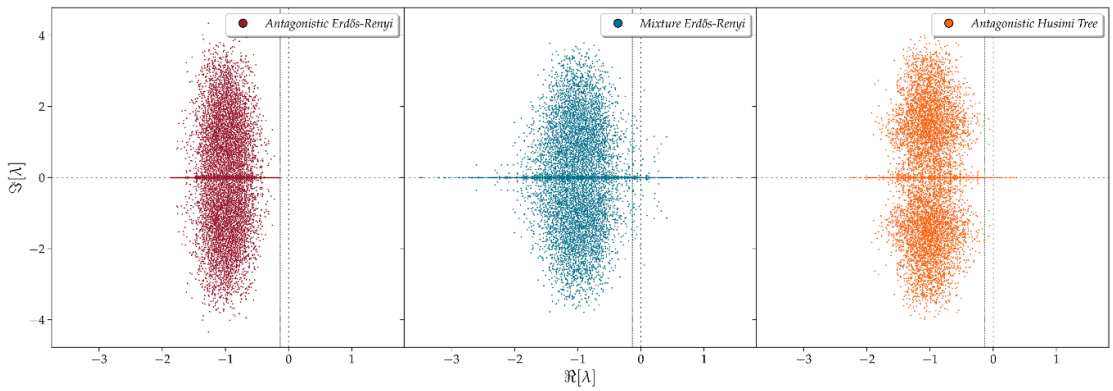

Figure 6. Spectra of Interaction-like matrices **B** for antagonistic Erdős–Rényi (red, left), mixture Erdős–Rényi (blue, centre) and antagonistic pure Husimi tree (orange, right). Markers denote the eigenvalues of a single matrix $\mathbf{B}_{\mathrm{Id}}$ of size $N = 8000$. The green dotted line displays $-D_{\min}$, the maximum diagonal entry of $\mathbb{B}$. The parameters used are those detailed in section 2.4.3.

This result is reminiscent of a related result for antagonistic tree graphs with fluctuating diagonal entries, which states that the leading eigenvalue of a interaction matrix associated with an antagonistic, tree graph is smaller or equal than $-D_{\min}$, see C.3. Figure 5 shows that the same principle applies for antagonistic, Erdős–Rényi graphs, and moreover, for the specific parameters chosen it holds that the leading eigenvalue of a large antagonistic Erdős–Rényi graph is approximately equal to the largest possible diagonal element $-d_{\min}$.

Note that $-d_{\min}$ does not always determine the leading eigenvalue of antagonistic Erdős–Rényi graphs. For example, let us consider the limiting case of a trivial diagonal with no disorder, i.e. $p_D(d) = \delta(d-1)$, as discussed in the previous section 4.1. The results of figure 3 show that $\langle \Re[\lambda_1] \rangle$ is larger than $-d_{\min} = -1$, and hence its value is not directly related to $d_{\min}$. Thus, depending on the model parameters, the asymptotic behaviour of the leading eigenvalue of antagonistic Erdős–Rényi graphs is either set to $-d_{\min}$ or it is determined by a complex interplay of various parameters.

In section 5, we will study the transition between these two regimes in more detail. Nevertheless, we emphasise that in both cases the real part of the leading eigenvalue converges to a finite value, marking a qualitative difference with respect to mixture Erdős–Rényi graphs and antagonistic Husimi trees.

At variance with shifted interaction matrices, we do not have theoretical results valid at infinite N to confirm that the numerical results for the antagonistic case converge to a finite value. However, note that the real part of the leading eigenvalue for the largest Ns observed converges to the upper boundary $-d_{\min}$ of the distribution of the elements on the diagonal (see in figure 5 the trend of the average $-D_{\min}$ for comparison), strongly suggesting that the right boundary of the spectrum on the real axis in the antagonistic case is simply determined by the disorder on the diagonal and therefore by definition does not diverge with N.

Figure 6 shows the full spectra of the matrices considered in figure 5. Comparing the spectra in figure 6 with those in figure 4, we observe again tails of eigenvalues on the real axis for the mixture Erdős–Rényi and antagonistic $(4, 4)$-pure Husimi tree ensemble. Note that in figure 6 we also observe a segment on the real axis in the spectrum of the antagonistic Erdős–Rényi graph. However, in the latter case, the segment of eigenvalues does not grow indefinitely as a function of N, and instead it is confined to the interval $[-d_{\max}, -d_{\min}]$, in agreement with the results in figure 5. Therefore, also for interaction-like matrices, strong LSS yields a finite segment of eigenvalues on the real axis[4] with direct consequences on the possibility to use strong LSS to predict structural stability and feasibility of models of ecosystems, irrespectively from system size, i.e. absolute stability.

Another difference between figures 4 and 6 is that in the latter we do not observe a reentrance effect in the spectrum of the antagonistic Erdős–Rényi graph. We stress however that this is due to the choice of model parameters, and that in general interaction-like matrices can also exhibit reentrance effects. In section 5, we will discuss in detail how reentrance effects appear in models with diagonal disorder, and how they depend on the model parameters.

4.3. Jacobian-like matrices J

Lastly, we investigate the validity of equation (37), on Jacobian-like matrices, $\mathbf{J} = \mathbf{D}\mathbf{B}_{\mathrm{Id}} = \mathbf{D}(\mathbf{A} - \mathbf{1})$, that have a distinctive stripy structure and negative diagonal, which is relevant for linear stability analysis in

[4] Note that in general if the distribution p_D is unbounded on $\mathbb{R}^+$, there will not be a finite segment of eigenvalues on the real axis, but the real part of the eigenvalues will still have a finite upper bound.

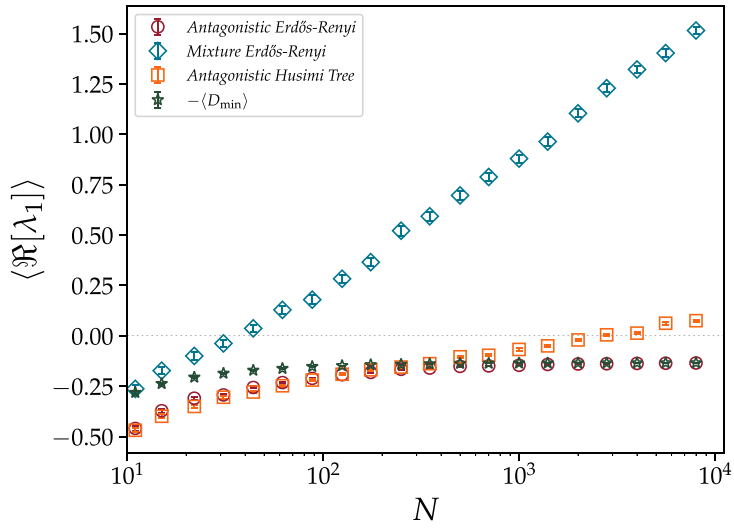

Figure 7. Average real part of the leading eigenvalue, $\langle \Re[\lambda_1]\rangle$, as a function of the matrix size N for Jacobian-like matrices $\mathbf{J}$. Results shown are for antagonistic Erdős–Rényi graphs (red circles), mixture Erdős–Rényi graphs (blue diamonds) and antagonistic pure Husimi trees (orange squares). The green stars are the averages of the largest element of the diagonal matrix $-D_{\min}$. Markers are sample means obtained from numerically diagonalising 300 matrix realisations, and error bars denote the error on the mean. The parameters used for the matrix ensembles are detailed in section 2.4.3.

ecology as explained in section 2. In order to have a negative diagonal, we extract the entries of the diagonal matrix $\mathbf{D}$ from a uniform distribution $p_D(d)$ supported on $[d_{\min}, d_{\max}]$, with $d_{\min} > 0$. Further details on the various parameters can be found in section 2.4.3.

Figure 7 depicts the average, real part of the leading eigenvalue, $\langle \Re[\lambda_1(\mathbf{J})]\rangle$, as a function of the matrix size N in the three canonical models of interest, mirroring the analysis in figures 3 and 5 (see more on this comparison in appendix E). The numerical results confirm the connection between strong LSS and finiteness of leading eigenvalue, viz., $\langle \Re[\lambda_1(\mathbf{J})]\rangle$ rapidly converges to a finite value for antagonistic, Erdős–Rényi graphs, while $\langle \Re[\lambda_1(\mathbf{J})]\rangle$ diverges as a function of N for mixture, Erdős–Rényi graphs and antagonistic, Husimi trees. In addition, in agreement with the results in figure 5 and 7 shows that for antagonistic Erdős–Rényi graphs the average leading eigenvalue saturates at a value that is approximately equal to $-D_{\min}$ (after a transient regime for small values of N). For antagonistic tree graphs, C.3 shows that the leading eigenvalue is smaller or equal than $-D_{\min}$. Figure 7 shows that this principle also applies to Jacobian-like matrices defined on antagonistic Erdős–Rényi graphs. Taken together, as discussed previously for the interaction like matrices, for the model under study the right boundary of the spectrum on the real axis in the antagonistic case is determined by the disorder on the diagonal and therefore by definition does not diverge with N.

In appendix F we refine the results of figure 7 for $\langle \Re[\lambda_1(\mathbf{J})]\rangle$ as a function of N, by considering the limit $d_{\min} \to 0$. In this limit, the antagonistic, Husimi tree exhibits strong transient effects, which we call the Husimi plateau. Nevertheless the results remain consistent with figure 7 as they eventually show a growth of $\langle \Re[\lambda_1(\mathbf{J})]\rangle$ with N. Note however that we do not expect that the conclusion about the finiteness of the boundary of the spectrum on the real axis at large N in the antagonistic Erdős–Rényi case could be just the result of a finite size effect in correspondence of a long Husimi-like plateau, because the Husimi plateau only forms for fine-tuned values of $d_{\min}$, while in the antagonistic Erdős–Rényi case the leading eigenvalue seems to always converge to a finite value as we could not observe any divergence for any choice of the $d_{\min}$ studied.

The results in figure 7 have interesting implications for the linear stability of ecosystems. Recalling the classical linear stability condition $\Re[\lambda_1(\mathbf{J})] < 0$, the results in figure 7 imply that system size N is not an important parameter for the linear stability of systems defined on strongly locally sign stable graphs, which therefore are absolutely stable. On the other hand, system size N is an important parameter in the general case of models defined on graphs with sign-symmetric interactions or with a number of short cycles growing with N, as in the latter cases stability is only attained for small enough values of N.

Figure 8 shows the spectra of Jacobian-like matrices for the three canonical models under study. The Jacobian-like spectra have an arrow-like shape, which resembles those already observed for the dense version of Jacobian-like matrices [60, 74]. However, importantly in the sparse case a clear distinction is observed between, on one hand, antagonistic Erdős–Rényi graphs, and on the other hand, mixture Erdős–Rényi graphs and antagonistic Husimi trees. The latter two exhibit long tails on the real axis that increase with system size, while the former does not exhibit such tails. Hence again, the divergence of the real part of the

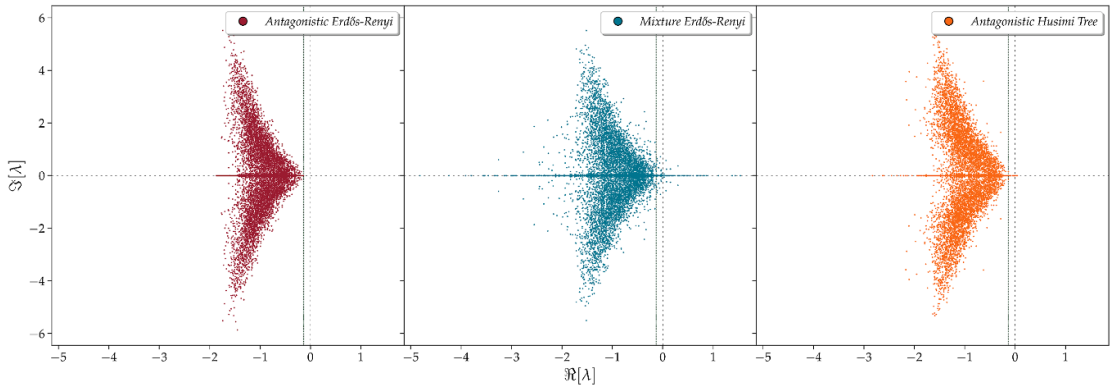

Figure 8. Spectra of a single realisation of Jacobian-like matrix **J** with size $N = 8000$ for antagonistic Erdős–Rényi (red, left), mixture Erdős–Rényi (blue, centre) and antagonistic pure Husimi tree (orange, right). The green dotted line displays $-D_{\min}$, the largest element of the diagonal matrix. The other parameters employed are discussed in section 2.4.3.

leading eigenvalue is due to tails that develop on the real axis of the spectra of sparse random graphs, and such tails are absent in strongly locally sign stable ensembles.

Note that the spectrum of the antagonistic, Erdős–Rényi graph in the left panel of figure 8 does not exhibit a reentrance effect, similar to the spectrum of the interaction-like matrix in the left panel of figure 6, but different from the spectrum of the shifted interaction matrix in the left panel of figure 4. We stress that this is due to the choice of model parameters, and in fact Jacobian-like matrices can also exhibit reentrance effects. In the next section we will investigate how reentrance in the spectra of Jacobian-like matrices is governed by an interplay between diagonal disorder and network structure.

5. Discontinuous transition in the imaginary part of the leading eigenvalue

As shown in the left panel of figure 4, the boundary of the spectrum of antagonistic Erdős–Rényi graphs exhibits a reentrance in correspondence of the real axis. In this case, the leading eigenvalue comes in a pair of complex conjugate values with finite imaginary part. From a dynamical systems point of view, the reentrance effect is interesting, as the imaginary part of the leading eigenvalue determines the frequency of oscillations of the slowest mode of relaxation towards the fixed point. Hence, if the leading eigenvalue has a nonzero imaginary part, then the leading, relaxation mode is oscillatory, while for leading eigenvalues that are real the leading mode is nonoscillatory. As a consequence, a transition from a phase in which the leading eigenvalue comes in a pair of two conjugate, complex values to a phase in which it is real corresponds, from a dynamical perspective, to a transition from an oscillatory to a nonoscillatory relaxation dynamics. For this reason we call it a *dynamical transition*.

Note that in general reentrance effects can be interesting both for interaction-like matrices and Jacobian-like matrices. In the latter, they identify oscillatory dynamics in nonlinear systems of the generalised Lotka–Volterra type in the vicinity of a fixed point. In the former, they may simply identify oscillatory dynamics of corresponding linear systems. However, for the generalised Lotka–Volterra model discussed in this paper, the dynamical behaviour is partially accessible by studying the Jacobian-like matrix only, and the reentrance effect visible in the spectrum of interaction-like matrix does not have any dynamical consequences. On the other hand, the emergence of a reentrance in the spectrum of the interaction-like matrix for the generalised Lotka–Volterra model can still represent an interesting piece of information in situations where the system is feasible/structurally stable, because the spectrum does not include the origin, although (complex) eigenvalues happen to have real parts of both positive and negative sign. In such cases the sign of the leading eigenvalue cannot directly determine structural stability or feasibility, as otherwise naively expected.

Antagonistic Erdős–Rényi graphs with constant diagonal entries, i.e. shifted interaction matrices, exhibit a dynamical transition as a function of the mean degree c, as shown in [25]. Indeed, for large c the boundary of the spectrum resembles the elliptic law, and thereby the leading eigenvalue is typically real in the large size limit. On the other hand, for small c the boundary of the spectrum shows a reentrance effect, as shown in the left panel of figure 4, and the leading eigenvalue is typically complex. In addition, [25] shows that the dynamical transition is a continuous transition in the following sense: the imaginary part $\Im[\lambda_1^\star]$ of the typical value $\lambda_1^\star$ of the leading eigenvalue, for which we provide a mathematical definition later, equals zero at the transition, and therefore the frequency of the oscillations near the transition is small.

In the present section, we also study the dynamical transition in the leading eigenvalue, but now for the interaction-like and Jacobian-like matrices with sign-antisymmetric weights. Note that in figures 6 and 8 we have not observed reentrance effects for interaction-like and Jacobian-like matrices, and consequently their leading eigenvalue is real. Instead, in figure 4 we have observed a reentrance in the spectra of shifted interaction matrices with sign-antisymmetric weights, and consequently in this case the leading eigenvalue comes in a pair of two conjugate, nonreal eigenvalues. Since the latter random matrix ensemble can be obtained from the former ensembles in the limit of small σ_D, a transition, possibly related to the reentrance of the spectra in correspondence of the real axis, is to be expected at intermediate values of σ_D.

Interestingly, the dynamical transition we find in this section for interaction-like and Jacobian-like matrices occurs while the spectrum is still reentrant in correspondence of the real axis, and hence it features a discontinuous jump in the imaginary part $\Im[\lambda_1^\star]$ of the leading eigenvalue, at variance with the nature of the transition studied in [25]. This section is devoted to a careful study of this transition. In particular, we further discuss the definition of a suitable control parameter for the transition, both in the interaction-like and Jacobian-like matrices, involving σ_D and other relevant parameters of the model. For both cases, in section 5.1 we locate the transition point through a finite size scaling analysis and in section 5.2, by some additional finite size scaling studies reported in appendix G, we also show that the transition takes place with a discontinuous jump.

5.1. Locating the transition point

As anticipated by the results of the previous section, a change in the strength of the diagonal disorder, as quantified by σ_D, can have a direct impact on the imaginary part of the leading eigenvalue of interaction-like and Jacobian-like matrices, determining a qualitative change in the relaxation dynamics of a corresponding dynamical system.

Concerning other model's parameter, in the interaction-like case, μ_D is only responsible of a global shift of the spectrum and cannot affect the imaginary part of the leading eigenvalue. A global rescaling of all matrix elements also affects trivially the spectrum. First non trivial changes in the spectrum emerge when σ_D changes with respect to the scale of the off-diagonal elements, represented by their variance σ, and therefore the relevant control parameter for the dynamical transition must be σ_D/σ[5].

For Jacobian-like matrices the situation is more involved as their off-diagonal elements are the result of the product of pairs of random variables D_i, A_{ij}, with probability distribution p_D and p. In this case, a global rescaling of the D_i gives also a trivial global rescaling of all the elements of the matrix. Any other modification of the parameters of p_D and p induces a non trivial modification of the probability distribution of the off-diagonal elements, which cannot be exactly recast in terms of the variation of a simple control parameter. However, it is possible to derive a rough estimate of the scale of the off-diagonal elements via their variance $\sigma_O = \sigma\sqrt{\mu_D^2 + \sigma_D^2}$, which suggests that the relevant control parameter is approximately given by the ratio $\sigma_D/\sigma_O = \sigma^{-1}/\sqrt{1 + \mu_D^2/\sigma_D^2}$.

We analyse in figure 9 the probability $P[\lambda_1 \in \mathbb{R}]$ that the leading eigenvalue is real as a function of the control parameters

$$s_B := \sigma_D/\sigma \quad \text{and} \quad s_J := \sigma_D/\sigma_O, \tag{39}$$

defined respectively for interaction-like and Jacobian-like matrices of antagonistic Erdős–Rényi graphs. For small values of s_B and s_J, $P[\lambda_1 \in \mathbb{R}] \approx 0.1$, and hence with high probability the leading eigenvalue has a nonzero imaginary part. On the other hand, for large values of s_B and s_J, $P[\lambda_1 \in \mathbb{R}] \approx 1$, and hence the leading eigenvalue is typically real. Because of the aforementioned dynamical significance of $\Im[\lambda_1]$, we call the former the *oscillatory phase* and the latter the *nonoscillatory phase*.

To show that the transition from an oscillatory to a nonoscillatory phase is a proper phase transition, we also plot in figure 9 the probability $P[\lambda_1 \in \mathbb{R}]$ for different system sizes N. Notably, the transition becomes sharper as the system size increases, and the curves for different values of N intersect at one single point, which we denote by s_d, indicating where the *dynamical transition* takes place. We also show results obtained at different values of σ, σ_D, μ_D, which all collapse when plotted as function of s_B and s_J. In particular, this evidence confirms that s_J can be effectively used as relevant control parameter for the transition[6].

[5] Additional non trivial modifications of the spectra are introduced by changes in the relative importance of μ_G and σ_G for fixed σ, as well as in general every change in the distribution of the diagonal and off-diagonal elements. Conversely, here we consider cases in which changes in σ are only obtained by changing both μ_G and σ_G, with μ_G/σ_G fixed.

[6] Be warned that for Jacobian-like matrix, s_J can be safely considered the relevant control parameter only as long as the modifications in the model parameters σ, μ_D, σ_D do not give rise to a significant change in the shape of the distribution of the off-diagonal elements when the transition takes place, as it is the case for the two series of data for the largest system size in the right panel of figure 9.

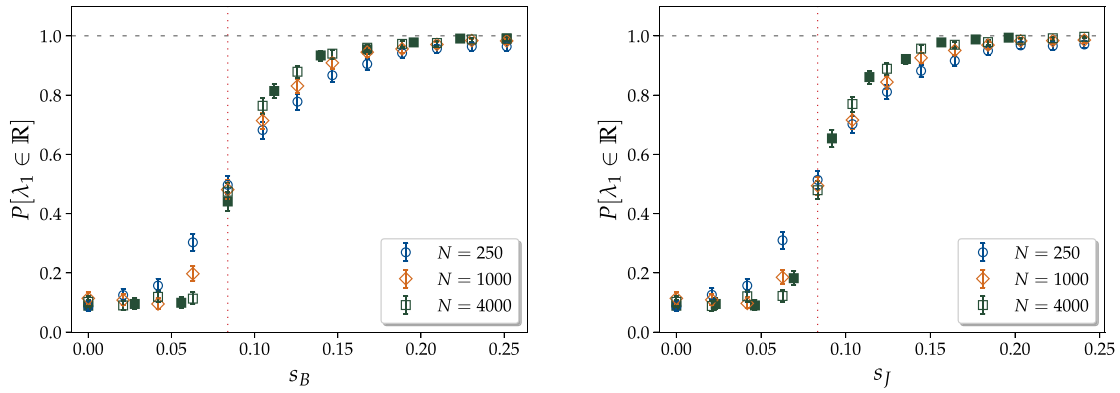

(a) Interaction-like **B** (b) Jacobian-like **J**

Figure 9. Probability $P[\lambda_1 \in \mathbb{R}]$ that the leading eigenvalue is real as a function of the control parameter, defined in equation (39), for interaction-like **B** (on the left) and Jacobian-like **J** (on the right) matrices of antagonistic Erdös–Rényi graphs. The vertical dotted line shows the value $s_d \simeq 0.08$ at which $P[\lambda_1 \in \mathbb{R}] \simeq 0.5$ and therefore indicates the transition from the complex phase to the real phase. Averages are performed over 1000 matrix realisations. The error bars depict the Wilson score interval at 95% confidence, which is an asymmetric interval that does not exhibit overshoot phenomena and does not underestimate the uncertainty around the endpoints, see [75–77]. The empty markers are obtained by employing the parameters discussed in section 2.4.3 and for given values of N, and the filled ones are obtained for parameters $\mu_G = 1.5$, $\sigma_G = 0.9$, $\mu_D = 1.2$, ten values of σ_D equally spaced in $[0, 0.45]$, and for $N = 4000$.

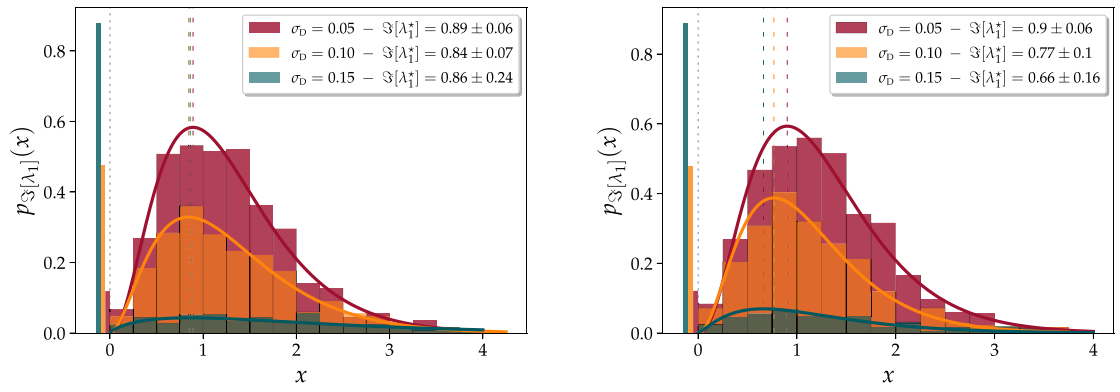

(a) Interaction-like **B** (b) Jacobian-like **J**

Figure 10. Histograms of the imaginary part of the leading eigenvalues of interaction-like **B** (on the left) and Jacobian-like **J** (on the right) matrices of antagonistic Erdös–Rényi graphs for $N = 4000$ and different values of the strength of the diagonal disorder: $\sigma_D = 0.05$ (corresponding to $s_B \simeq 0.04$ and $s_J \simeq 0.04$) in red, $\sigma_D = 0.10$ (corresponding to $s_B \simeq 0.08$ and $s_J \simeq 0.08$) in orange, and $\sigma_D = 0.15$ (corresponding to $s_B \simeq 0.13$ and $s_J \simeq 0.12$) in green; the other parameters employed are as discussed in section 2.4.3. The solid lines are γ-distributions fitted to the histograms (see main text for detailed explanations), and the dashed vertical lines denote the mode of these fitted distributions, which provide the estimates for $\Im[\lambda_1^\star]$. The delta peaks in zero denote the probability $P[\lambda_1 \in \mathbb{R}]$ that an eigenvalue is real.

Note that in the oscillatory phase $P[\lambda_1 \in \mathbb{R}] \approx 0.1$ for large values of N, and hence there is a small nonzero probability that the leading eigenvalue is real. Hence, the imaginary part of the leading eigenvalue is not a self-averaging quantity (i.e. it does not converge to a deterministic number in the infinite size limit), which is in correspondence with the numerical results from [25].

5.2. Characterising the discontinuity of the transition

In this section, we determine whether the dynamical transition occurs with a continuous or discontinuous variation of the imaginary part of the leading eigenvalue.

Figure 10 displays the distribution $p_{\Im[\lambda_1]}(x)$ of the imaginary parts of the leading eigenvalue obtained by generating a large sample of interaction-like matrices **B** (left panel) and Jacobian-like matrices **J** (right panel); notice that for each pair of conjugate leading eigenvalues with nonzero imaginary part we only focus on the one with $\Im[\lambda_1] > 0$. From figure 10, we observe that the distribution $p_{\Im[\lambda_1]}(x)$ consists of two parts, viz., a

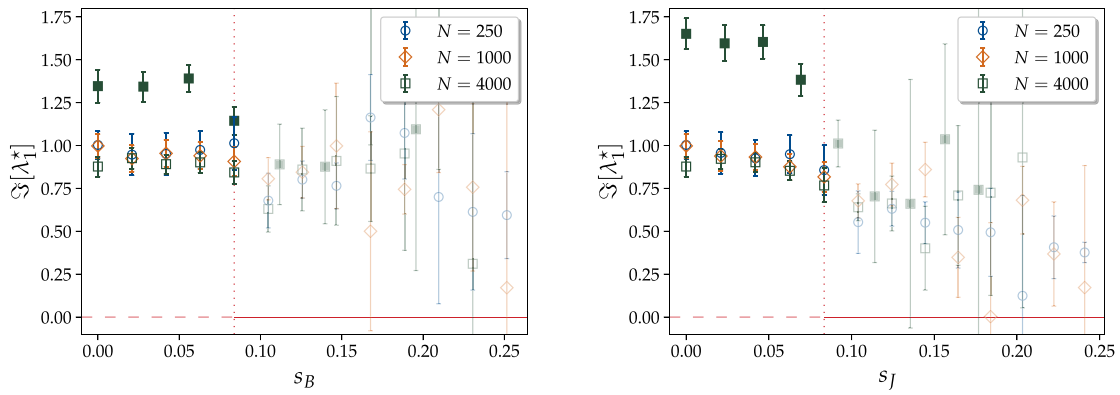

(a) Interaction-like **B** (b) Jacobian-like **J**

Figure 11. Imaginary part $\Im[\lambda_1^\star]$ of the typical, nonreal, leading eigenvalue as a function of the control parameters, as defined in equation (39), for interaction-like **B** (on the left) and Jacobian-like **J** (on the right) matrices of antagonistic Erdös–Rényi graphs. The values of $\Im[\lambda_1^\star]$ are estimated as shown in figure 10, viz., as the mode of a γ-distribution fitted to a histogram built out of 1000 matrix realisations. The error bars are computed by standard error propagation from the fitting parameters. The parameters employed for empty and filled markers are the same as those used in figure 9, respectively. The vertical dotted line depicts the transition value s_d. Note that the markers after the transition are denoted in a lighter shade because they represent data which are merely the result of finite size effects: in the nonoscillatory phase the frequency of complex leading eigenvalues decreases with system size. After the transition the eigenvalues are instead typically real, as represented by the solid red line ($\Im[\lambda_1^\star] = 0$). Its left dashed continuation shows rare real leading eigenvalues also present in the oscillatory phase.

delta distribution at zero carrying the fraction $P[\lambda_1 \in \mathbb{R}]$ of matrix realisations that have a real-valued leading eigenvalue, and a continuous distribution corresponding with eigenvalues that have nonzero imaginary part:

$$p_{\Im[\lambda_1]}(x) = P[\lambda_1 \in \mathbb{R}]\,\delta(x) + (1 - P[\lambda_1 \in \mathbb{R}])\,\tilde{p}_{\Im[\lambda_1]}(x)\,. \tag{40}$$

We define

$$\Im[\lambda_1^\star] := \mathrm{argmax}_{x \in \mathbb{R}^+}\, \tilde{p}_{\Im[\lambda_1]}(x)\,, \tag{41}$$

as the typical value of the imaginary part of the leading eigenvalue.

As the control parameter changes from $s < s_\mathrm{d}$, to $s \approx s_\mathrm{d}$ and to $s > s_\mathrm{d}$ (obtained for $\sigma_D = 0.05$, $\sigma_D = 0.10$ and $\sigma_D = 0.15$ in correspondence of $\sigma_\mathrm{G} = 0.6$ and $\mu_\mathrm{G} = 1.0$) it can be observed that the maximum of the continuous part of the distribution, indicated by the vertical dashed line, is mostly independent on the control parameter both for interaction-like and Jacobian-like matrices. The change in the control parameters mainly affects the weight $P[\lambda_1 \in \mathbb{R}]$ carried by the two parts of the distribution $p_{\Im[\lambda_1]}(x)$, as it is usual with discontinuous phase transitions and at variance with the continuous dynamical transition found in [25] for shifted interaction matrices as a function of c. Since the numerical results in figure 10 are obtained at finite N, we perform in appendix G a detailed, finite size scaling analysis of the distribution $p_{\Im[\lambda_1]}(x)$, which confirms that the discontinuity in $\Im[\lambda_1^\star]$ at the transition is to be expected also in the large N limit.

Following the approach implemented in [25], to get an estimate of the typical value, $\Im[\lambda_1^\star]$, of the portion of the distribution corresponding to nonzero imaginary part we take the mode of a γ-distribution $\gamma(x;\alpha,\beta) = \frac{\beta^\alpha x^{\alpha-1} e^{-\beta x}}{\Gamma(\alpha)}$ fitted on the histogram of $\Im[\lambda_1] > 0$. Here $\Gamma(\alpha)$ is the gamma function with parameters $\alpha, \beta \in \mathbb{R}^+$ real and positive.

The typical value $\Im[\lambda_1^\star]$ for different sizes N is plotted in figure 11 as a function of the control parameter for the interaction-like and Jacobian-like case and with the same settings as in figure 9. As it can be observed again, $\Im[\lambda_1^\star]$ is an almost constant function of the control parameter and its value at the transition point is positive until it vanishes at s_d, showing the discontinuous nature of the transition and the associated finite size effects. For further evidence, the lighter markers show that $\Im[\lambda_1^\star]$ is nonzero also in the nonoscillatory phase (the dynamical transition point is indicated by the vertical dotted line) when the leading eigenvalue is typically real. Finally, notice that while the location of the transition is only controlled by s_B or s_J, respectively, the value of $\Im[\lambda_1^\star]$ depends on the particular choice of the model parameters. This value reflects the global rescaling of the matrix as discussed at the beginning of section 5.1.

Lastly, to develop a better understanding about the mechanism of the discontinuity in the dynamical transition of interaction-like and Jacobian-like matrices, we investigate their spectra in figures 12 and 13 at

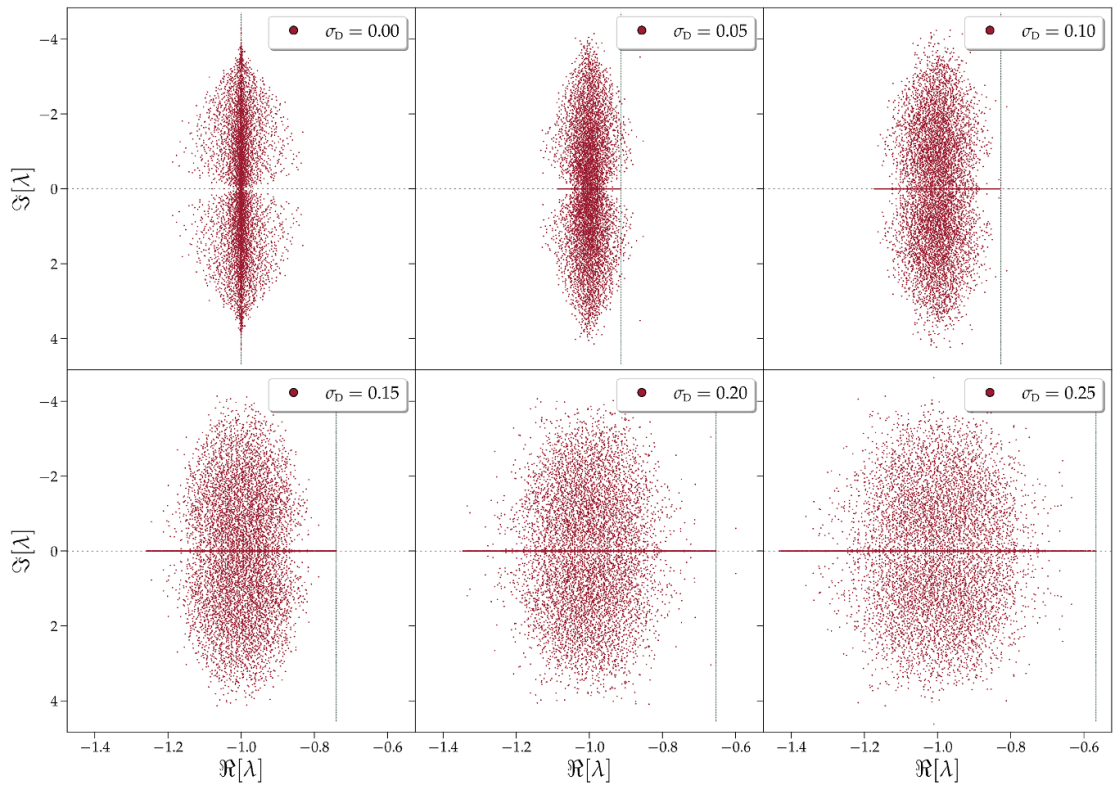

Figure 12. Spectra of single realisations of antagonistic, Erdős–Rényi, interaction-like matrices $\mathbf{B} = \mathbf{A} - \mathbf{D}$ of size $N = 8000$. The diagonal entries of $\mathbf{D}$ are drawn from a uniform distribution with σ_D as depicted in the legend, corresponding to values of $s_B = 0$, $s_B \simeq 0.4$, $s_B \simeq 0.8$, $s_B \simeq 0.13$, $s_B \simeq 0.17$ and $s_B \simeq 0.21$ (left to right, up to bottom). The green dotted line displays $-D_{\min}$. The other parameters employed are as discussed in section 2.4.3.

different values of the control parameters. Let us first discuss the spectra of antagonistic, interaction-like matrices in figure 12. We observe that the spectrum contains two parts, viz., a cloud of eigenvalues that have a nonzero imaginary part and a segment of real-valued eigenvalues. In particular, the width of the segment of real eigenvalues is approximately equal to $[-D_{\max}, -D_{\min}]$, and hence the segment width increases as a function of σ_D (or as a function of s_B, for fixed σ). The discontinuous nature observed for the dynamical transition is originated from the competition between the width of the cloud of complex eigenvalues and the width of the segment on the real axis. It can be observed that for $s_B < s_{\rm d}$, the leading eigenvalue belongs to the cloud of complex eigenvalues, and since the shape of this cloud is reentrant the imaginary part of the leading eigenvalue in this regime is nonzero. On the other hand, for $s_B > s_{\rm d}$, the leading eigenvalue belongs to the segment of real eigenvalues, and hence has null imaginary part. Since the eigenvalue cloud is still reentrant at the point $s_B = s_{\rm d}$ when the segment width overtakes the width of the cloud, the transition is discontinuous. This behaviour is different from the continuous transition driven by the connectivity c at $s_B = 0$, as discussed in [25]. In this case, the transition in the imaginary part of the leading eigenvalue is the result of a gradual reshaping of the spectrum resulting in the progressive disappearance of the reentrance in correspondence of the real axis at large c.

For the spectra of Jacobian matrices, shown in figure 13, the qualitative picture is similar to what we have discussed for figure 12 for interaction-like matrices, viz., the spectrum consists of two parts, one being a cloud of complex eigenvalues reentrant in correspondence of the real axis and the other is a segment of real eigenvalues approximately supported on $[-D_{\max}, D_{\min}]$. Again, a discontinuous transition on the imaginary part of the leading eigenvalue takes place as the cloud of eigenvalue is reentrant when the width of the segment overtakes the width of the cloud of eigenvalues.

In both cases, in the nonoscillatory phase, $\Re[\lambda_1] \approx -D_{\min}$, as the support of the real eigenvalues is well approximated by $[-D_{\max}, -D_{\min}]$, which is consistent with the results in figures 5 and 7.

Moreover, in both cases, it emerges that the reentrance of the cloud of complex eigenvalue in correspondence of the real axis also becomes slightly less pronounced if σ_D increases, which hints to the possibility that, for specific settings, the disappearance of the reentrance could take place before the largest real eigenvalues become the leading one. In such situation a continuous transition of the imaginary part of the leading eigenvalue is to be expected, instead of the discontinuous transition observed here. In general, by

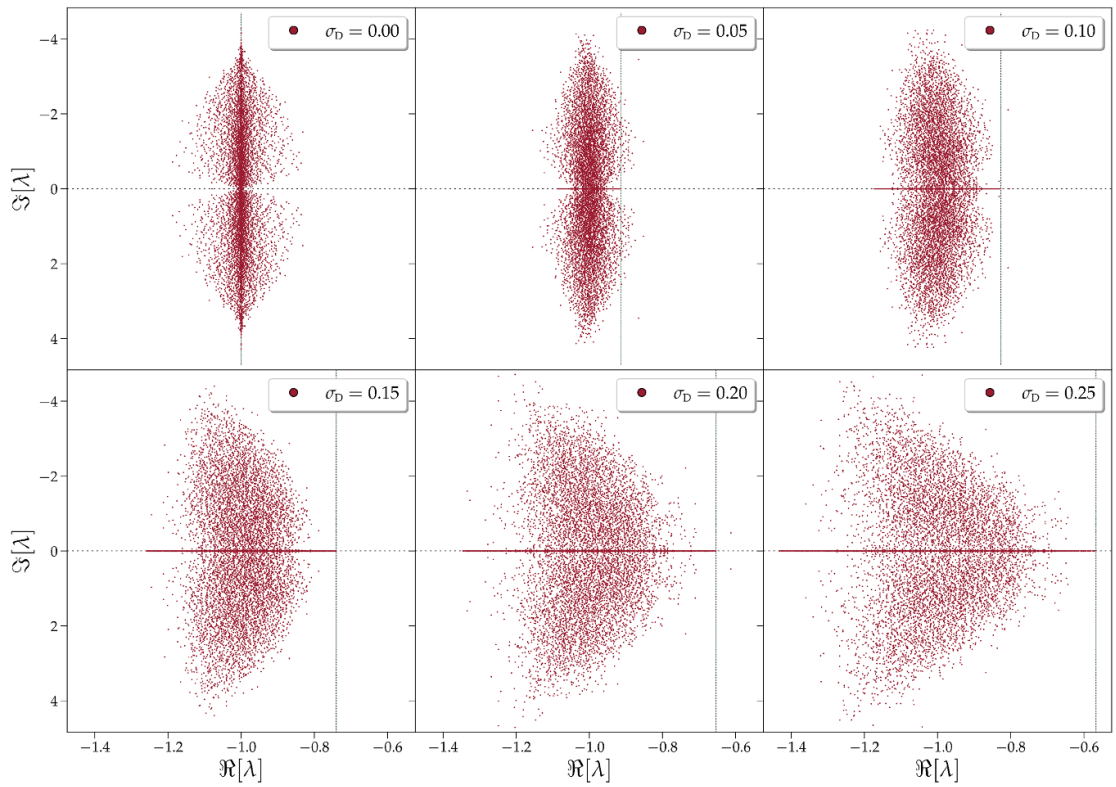

Figure 13. Spectra of single realisations of antagonistic, Erdős–Rényi, Jacobian-like matrices $\mathbf{J} = -\mathbf{D}\mathbf{B}_{\mathrm{Id}}$ of size $N = 8000$. The diagonal entries of $\mathbf{D}$ are drawn from a uniform distribution with σ_D as depicted in the figure legends, corresponding to values $s_J = 0$, $s_J \simeq 0.4$, $s_J \simeq 0.8$, $s_J \simeq 0.12$, $s_J \simeq 0.16$ and $s_J \simeq 0.20$ (left to right, up to bottom). The green dotted line displays $-D_{\mathrm{min}}$. The other parameters employed are as discussed in section 2.4.3.

modifying the parameters contained in the distributions p and p_D and the connectivity of the graph, it should be possible to obtain a phase diagram containing a line of discontinuous transition ending in a continuous transition point. This interesting endeavour is left for future work. Finally, there is one notable distinction between figures 12 and 13, namely, for large values of σ_D the spectra of interaction-like matrices have a round shape, albeit not circular, while the spectra of Jacobian-like matrices has a characteristic arrow shape, which has also been observed before for dense matrices, see [60, 74]. This different behaviour can produce a qualitative difference in the phase diagram containing discontinuous and continuous dynamical transitions of interaction-like and Jacobian-like matrices, which will be also interesting to study.

6. Discussion

In this paper, we have focused on two interesting features of the spectra of sparse random graphs. First, we have analysed how the leading eigenvalue of random graphs depends on the system size, taking into account the sign pattern of matrix entries and the graph topology. Second, we have studied how the imaginary part of the leading eigenvalue transitions from zero to a nonzero value as a function of the model parameters in the large system limit. These features are specific to sparse network topologies and do not appear in highly connected graphs.

More specifically, this paper presents a simple, general criterion for predicting the asymptotic behaviour of the leading eigenvalue of infinitely large, sparse, random graphs, based on the concept of strong local sign stability. Although in some previous examples ([21, 25]) the importance of the sign pattern and network topology on the stability of some matrices was emerging, here we also systematically investigate the validity of the proposed criterion with additional numerical examples on sparse random graphs with different topologies and sign patterns, and for different types of matrices such as adjacency matrices and Jacobian-like matrices.

Aside the numerical evidence, we can also provide an intuitive explanation for the relation between strong local sign stability and the finiteness of the real part of the leading eigenvalue within the context of linear, dynamical system defined on a strongly locally sign stable graph. For locally sign stable graphs, when a perturbation is applied to a random node its neighbours react. However typically the finite neighbourhood is, by definition, stable, therefore the perturbation will be damped. This scenario could, in principle, be

overturned by cycles of length $O(\log(N))$ that break sign stability, but since they are long we do not expect their effect to be strong enough to destabilise the system in all cases. The situation is different for large, random graphs that are not locally sign stable. In such graphs there exist nodes that are not locally stable, and hence perturbations applied to these nodes will always locally grow and destabilise the system. In addition, whenever the random graph is locally sign stable but not strongly locally sign stable and short cycles are growing in number with system size, there may exist few nodes that belong to a large number of short cycles and lead again to a local instability.

One very interesting feature of strong local sign stability, following from the concept of sign stability, is that it is not affected by the absolute values of the matrix elements and thus it refers to the set of graphs with the same network topology and sign pattern, provided that the distribution of the off-diagonal elements has finite second moment. As a consequence, whenever the interaction matrix **A** of an ecosystem is strongly locally sign stable, then also the corresponding interaction-like **B** and Jacobian-like **J** matrices are strongly locally sign stable, potentially ensuring at once feasibility, structural stability and linear stability. This aspect is particularly interesting in the ecological context where, as anticipated in the Introduction, it is difficult to quantify the strength of interactions between species [2, 36]. In this regard, [29] has shown that for a general predator–prey model defined on a tree, the Jacobian matrix (with negative elements on the diagonal) evaluated on an isolated, feasible equilibrium point has eigenvalues with negative real parts, and hence the equilibrium point is linearly stable for such systems. The concept of strong local sign stability that we have introduced in the present paper generalises the results in [29], as it applies to a broader class of systems, including predator–prey ecosystems defined on random graphs that are locally tree-like, have a finite number of short cycles, and have diagonal elements that are negative and below a finite threshold. The last condition is needed to have all eigenvalues with negative real part despite the finite width of the spectrum.

Our results challenge the classical notion that complex, dynamical systems exhibit a trade-off between size and stability, mostly discussed for fully connected models [10, 11, 36, 51, 78]. Indeed, in dense graphs the sign pattern does not alter how the leading eigenvalue scales with system size [11, 61, 64]. Instead, for sparse graphs we find that this trade-off depends on the sign pattern and topology of the graph. More specifically, [25] showed that the real part of the leading eigenvalue of infinitely large, antagonistic Erdős–Rényi graphs with shifted interaction matrix is finite, also by means of theoretical predictions on the boundary of the spectrum in the limit $N \to \infty$. The present work generalises this result with numerical evidences by extending it to various matrix structures relevant in ecology and by identifying the common feature the convergence of the real part of the leading eigenvalue to a finite value for large system size. It will be interesting to extend the theoretical predictions from interaction-like matrices [25] to more general matrices to put on a firmer grounds the extrapolation of numerical results to infinite N. In general it is also interesting to consider models for which the fraction of sign-symmetric interactions is vanishing with N, or antagonistic models defined on graphs with power law degree distribution, which are locally sign stable but not strongly locally sign stable (due to a growing number of finite cycles albeit a vanishing fraction of them), to understand whether the conditions to grant finite leading eigenvalue can be relaxed.

It is important to emphasise that the strong LSS criterion (37) applies to matrices built from graphs as explained in section 2.4, i.e. without correlations among network topology, sign pattern and interaction weights. In fact, including correlations between network topology and interaction weights, the leading eigenvalue can diverse with the system size even though the graph is strongly LSS. As an example, consider a sequence $\mathbf{M}_N$ in which the two entries with the largest absolute values concentrate with the same sign on the same edge, say $M_{12} = \max_{i,j}\left\{|M_{ij}| : i,j \in V\right\}$ and $M_{21} = \max_{i,j}\left\{|M_{ij}| : i,j \in V\right\} \setminus \{M_{12}\}$. If the entries are also drawn from a distribution with unbounded support, these largest values M_{12} and M_{21} diverge as a function of N. Then in the limit of large N, the leading eigenvalue $\lambda_1 \approx \sqrt{M_{12}M_{21}}$ and thus it diverges as a function of the system size N. At the same time, since we are only imposing the weights of a single edge the sequence $\mathbf{M}_N$ may still be strongly locally sign stable. Another possible example is a graph in which the node with the largest degree has all sign-symmetric edges. Also in this case, as long as the degree distribution has unbounded support, the leading eigenvalue diverges with the system size N, although the graph may be strongly locally sign stable.

Systematic studies of the stability properties of sparse systems are far from being achieved, although potentially relevant for many applications of dynamical systems. In particular new interest is arising on the rich phenomenology of sparse ecosystems [62]. We believe that our paper gives an important contribution by grasping a general criterion for stability of sparse ecosystems.

The second main result presented in this paper concerns the imaginary part of the leading eigenvalue $\Im[\lambda_1]$ of antagonistic Erdős–Rényi graphs. The spectra of antagonistic Erdős–Rényi interaction-like and Jacobian-like matrices display a transition driven by the strength of the diagonal disorder σ_D from a low σ_D-phase in which the leading eigenvalue typically has nonzero imaginary part to a large σ_D-phase in which

it is real. In the first phase the spectrum is characterised by a reentrance effect around the real axis and this is the cause for it to have a pair of complex conjugate leading eigenvalues.

This reentrance effect is specific to sparse, low connectivity graphs with sign-antisymmetric weights. In fact, as soon as we move away from the low connectivity limit the spectra tend, under fairly general conditions, to have an elliptic shape. It is worth noting that the spectral reentrance observed in sparse random graphs is a qualitatively new feature, which has only been previously observed in the recent work [25]. That paper identifies a transition in the spectra of antagonistic Erdős–Rényi graphs with zero diagonal entries driven by the connectivity c, from a large c phase where $\Im[\lambda_1] = 0$ to a small c phase where typically $\Im[\lambda_1] \neq 0$, and which also displayed a reentrance effect. The present paper generalises this result by extending it to more elaborate matrix structures. In particular, we have shown that the reentrance effect persists even in the presence of a disordered diagonal or a stripy, Jacobian-like, structure, but only as long as their disorder is not too large.

It is important to stress once more that while the transition described in [25] is continuous, the one discussed in the present paper is discontinuous. In the former case, the reentrance disappears progressively as the connectivity increases. On the other hand, in the latter case, the spectrum is composed of a cloud of complex eigenvalues and of a segment lying on the real axis. In the low σ_D phase, the leading eigenvalue is determined by the cloud and is therefore complex. As σ_D increases, both of these components gradually change: the cloud reshapes, reducing the reentrance effect, while the real segment elongates. At the transition, the right tip of the real segment reaches the convex hull of the cloud, and the leading eigenvalue starts to be real. This overtaking occurs before the reentrance has completely disappeared, and therefore we observe a jump in the leading eigenvalue imaginary part, giving rise to a discontinuous transition. At the same time it is possible that, for specific settings, the reentrance effect could disappear completely before (or together with) the overtaking by the segment on the real axis thus making the transition continuous. A more detailed study of the phase diagram describing both the reentrance effect and the transition in $\Im[\lambda_1]$ is left for future work. Moreover, since this reentrance effect is peculiar to sparse graphs, we expect the network topology to be relevant and therefore it would be interesting to investigate its impact.

The transition in $\Im[\lambda_1]$ discussed in this paper, especially with regard to Jacobian-like matrices, is of interest in the context of dynamical systems. In this framework, the imaginary part of the Jacobian leading eigenvalue determines the oscillation frequency of the slowest mode of relaxation towards the related fixed point. Accordingly, the response to a perturbation around a fixed point is oscillatory if the leading eigenvalue has imaginary part different from zero, nonoscillatory otherwise. Our result on the transition indicates that the dynamical response of a nonlinear system defined on antagonistic Erdős–Rényi is oscillatory only if the strength of the diagonal disorder σ_D is small compared to the off-diagonal one σ_O.

In order to appreciate the actual implication of this dynamical transition it would be interesting to derive a phase diagram describing the dynamical behaviours of antagonistic systems defined on sparse graphs. Indeed, in the context of dynamical systems with nonsymmetrical interactions the spectra of Jacobian matrices can play a role only in the case in which the dynamics is attracted by fixed points while chaos and limit cycles are not predominant. In dense ecological models such a phase diagram has been derived and it identifies regions with multiple attractors where solutions are often chaotic [79–82]. An analogous phase diagram for sparse ecosystems with predator–prey interactions is not known and its derivation is an interesting endeavour left for future work.

Finally, concerning applications, our findings on the importance of strong local sign stability in enhancing stability are consistent with empirical observations on real food webs, which are graphs that represent predator–prey interactions in ecological systems. According to our results, locally tree-like structures and sign-antisymmetric interactions stabilise large ecosystems, and hence, these are the structures we expect to observe. Empirical studies have shown that food webs are indeed locally tree-like, with a number of cycles that is similar to those found in locally tree-like Erdős–Rényi graphs [83]. Notably, other networks such as social and technological networks have a significantly larger number of cycles, a feature unique to food webs [83]. In addition, [84] found that the weights of long cycles in real food webs are typically smaller than in random matrices, further underlying the importance of locally tree-like structures for large ecosystems.

Data availability statement

The data cannot be made publicly available upon publication because they are not available in a format that is sufficiently accessible or reusable by other researchers. The data that support the findings of this study are available upon reasonable request from the authors.

Acknowledgment

We thank Andrea Marcello Mambuca for insightful discussions at the initial stage of this work. This work was also supported by the Simons Foundation Grant on Cracking the Glass Problem (#454935 Giulio Biroli).

Appendix A. Structural stability to perturbations of various ecological parameters

In this appendix we derive the expression for structural stability, defined as the stability of the abundances of surviving species $\vec{N}^*$, as defined in equation (10), with respect to small perturbations of the three different ecological parameters of our model r_i, K_i and α_{ij}. In particular, we show that in all three cases the susceptibility of $\vec{N}^*$ to perturbations of ecological parameters is related to the inverse of the matrix $\mathbf{B}$, defined in equation (11) and therefore it is singular if the spectrum of $\mathbf{B}$ contains the origin of the complex plane.

Let's start with the simplest case of a perturbation applied to the growth rates $r_i \to r_i + \xi_i$. The perturbed equations for the N_i^* then read

$$r_i + \xi_i = \frac{N_i^*}{K_i} + \sum_{j=1;j\neq i}^{S} \alpha_{ij} N_j^* \,, \tag{A.1}$$

which can be derived with respect to ξ_k

$$\delta_{ik} = \frac{1}{K_i}\frac{\partial N_i^*}{\partial \xi_k} + \sum_{j=1;j\neq i}^{S} \alpha_{ij}\frac{\partial N_j^*}{\partial \xi_k} = \sum_{j=1}^{S} B_{ij}\frac{\partial N_j^*}{\partial \xi_k} \,, \tag{A.2}$$

revealing that the susceptibility of N_i^* to little variations of r_k is directly determined by the inverse of $\mathbf{B}$:

$$\frac{\partial N_i^*}{\partial \xi_k} = \left(\mathbf{B}^{-1}\right)_{ik} \,. \tag{A.3}$$

Let's now consider a perturbation applied to the parameter $K_i \to K_i + \eta_i$, after which the perturbed equations for the N_i^* read

$$r_i = \frac{N_i^*}{K_i + \eta_i} + \sum_{j=1;j\neq i}^{S} \alpha_{ij} N_j^* \,. \tag{A.4}$$

Deriving with respect to η_k and evaluating the derivative at $\vec{\eta} = 0$

$$0 = -\delta_{ik}\frac{N_i^*}{K_i^2} + \sum_{j=1}^{S}\left(\frac{\delta_{ij}}{K_i} + \alpha_{ij}\right)\frac{\partial N_j^*}{\partial \eta_k} = -\delta_{ik}\frac{N_i^*}{K_i^2} + \sum_{j=1}^{S} B_{ij}\frac{\partial N_j^*}{\partial \eta_k} \,, \tag{A.5}$$

we find the susceptibility of N_i^* to little variations of K_k which is determined the inverse of $\mathbf{B}$ multiply row-by-row by $\frac{N_k^*}{K_k^2}$:

$$\left.\frac{\partial N_i^*}{\partial \eta_k}\right|_{\vec{\eta}=0} = \left(\mathbf{B}^{-1}\right)_{ik}\frac{N_k^*}{K_k^2} \,. \tag{A.6}$$

Finally we consider a perturbation applied to the interaction $\alpha_{ij} \to \alpha_{ij} + \epsilon_{ij}$ which lead to

$$r_i = \frac{N_i^*}{K_i} + \sum_{j=1;j\neq i}^{S}\left(\alpha_{ij} + \epsilon_{ij}\right) N_j^* \,. \tag{A.7}$$

Deriving with respect to ϵ_{kl} and evaluating the derivative at $\epsilon_{kl} = 0 \;\; \forall \;\; k \neq l$

$$0 = \sum_{j=1}^{S}\left(\frac{\delta_{ij}}{K_i} + \alpha_{ij}\right)\frac{\partial N_j^*}{\partial \epsilon_{kl}} + N_l^*\delta_{ik} = \sum_{j=1}^{S} B_{ij}\frac{\partial N_j^*}{\partial \epsilon_{kl}} + N_l^*\delta_{ik} \,, \tag{A.8}$$

we find the susceptibility of N_i^* to little variations of α_{kl} which is again related to the inverse of $\mathbf{B}$:

$$\left.\frac{\partial N_i^*}{\partial \epsilon_{kl}}\right|_{\epsilon=0} = -\left(\mathbf{B}^{-1}\right)_{ik} N_l^* \,. \tag{A.9}$$

In conclusion, a singular behaviour emerges if the spectrum of $\mathbf{B}$ contains the origin of the complex plane hinting to a large susceptibility of the solution of $\vec{N}^*$ to all three ecological parameters.

Appendix B. The eigenvalues of antagonistic trees have zero real part

We show that the adjacency matrices $\mathbf{M} \in \mathbb{R}^{N\times N}$ of trees weighted with sign-antisymmetric interactions have purely imaginary eigenvalues, i.e.

$$\Re\left[\lambda_i\right] = 0 \tag{B.1}$$

for all $i = 1, 2, \ldots, N$. As interactions are sign-antisymmetric, it holds that

$$M_{ij} M_{ji} < 0 \tag{B.2}$$

for all pairs (i, j) for which either $M_{ij} \neq 0$ or $M_{ji} \neq 0$. The tree condition implies that equation (35) holds. We assume that $M_{ii} = 0$.

The arguments we present are adapted from [3], albeit applied to the case of antagonistic, tree graphs.

First we define a general class of, so-called, strictly quasi-antisymmetric matrices, and we show that these matrices have purely imaginary eigenvalues. Second, we show that antagonistic trees are strictly quasi-antisymmetric.

B.1. Eigenvalues of strictly quasi-antisymmetric matrices are imaginary

We say that a matrix $\mathbf{Q} \in \mathbb{R}^{N\times N}$ is strictly quasi-antisymmetric if

$$\mathbf{Q}^{\mathrm{T}} = -\boldsymbol{\eta}\mathbf{Q}\boldsymbol{\eta}^{-1}, \tag{B.3}$$

where $\boldsymbol{\eta}$ is a symmetric, positive definite matrix; notice that [85, 86] define strictly quasi-symmetric matrices, which are related to PT-symmetric matrices in quantum mechanics [87].

Strictly quasi-antisymmetric matrices have imaginary eigenvalues as they are similar to an antisymmetric matrix $\mathbf{K}$. Indeed, since $\boldsymbol{\eta}$ is positive and symmetric, it is a diagonalisable matrix with positive eigenvalues. We define $\sqrt{\boldsymbol{\eta}}$ as the square root of $\boldsymbol{\eta}$ that is positive definite, which is the (unique) symmetric, matrix that has eigenvalues that are equal to the positive square roots of the eigenvalues of $\boldsymbol{\eta}$. Consequently, we may define the matrix

$$\mathbf{K} = \sqrt{\boldsymbol{\eta}}\mathbf{Q}\sqrt{\boldsymbol{\eta}}^{-1}, \tag{B.4}$$

which has real-valued entries as $\sqrt{\boldsymbol{\eta}}$ has real-valued entries. The matrix $\mathbf{K}$ is antisymmetric, as

$$\mathbf{K} = \sqrt{\boldsymbol{\eta}}\mathbf{Q}\sqrt{\boldsymbol{\eta}}^{-1} = \sqrt{\boldsymbol{\eta}}^{-1}\boldsymbol{\eta}\mathbf{Q}\boldsymbol{\eta}^{-1}\sqrt{\boldsymbol{\eta}} = -\sqrt{\boldsymbol{\eta}}\mathbf{Q}^{\mathrm{T}}\sqrt{\boldsymbol{\eta}} = \left(\sqrt{\boldsymbol{\eta}}\mathbf{Q}\sqrt{\boldsymbol{\eta}}\right)^{\mathrm{T}} = -\mathbf{K}^{\mathrm{T}}\,, \tag{B.5}$$

where in the last step we have used that $\sqrt{\boldsymbol{\eta}}$ is a symmetric matrix. Hence, since $\mathbf{Q}$ is similar to $\mathbf{K}$, both matrices share the same eigenvalues [71], and since $\mathbf{K}$ is an antisymmetric with real-valued entries, the eigenvalues of $\mathbf{Q}$ are purely imaginary.

B.2. Adjacency matrices of trees with sign-antisymmetric weights are strictly-quasi-antisymmetric

We show that the adjacency matrices $\mathbf{M}$ of antagonistic trees are strictly quasi-antisymmetric i.e. they satisfy equation (B.3). To this aim, following [3], we explicitly construct the matrix $\boldsymbol{\eta}$.

We select a random node in the graph, which we call the root node, and we label it as i_0. Subsequently, we consider (i) the set of nodes V_1 that are neighbours of i_0; (ii) the set of nodes V_2 that are neighbours of nodes in V_1 excluding the root node; (iii) the set of nodes V_3 that are neighbours of V_2 and are not part of V_1, etc. Eventually we obtain a partitioning $V = \{i_0\} \cup V_1 \cup V_2 \cup \ldots V_\ell$ of the set of vertices of the tree graph $G = (V, E)$ associated with $\mathbf{M}$, where ℓ is the depth of the tree rooted at i_0.

The matrix $\boldsymbol{\eta}$ is a diagonal matrix with elements on the diagonal defined as follows. We set the matrix entry associated to the root node to unity,

$$\eta_{i_0 i_0} = 1, \tag{B.6}$$

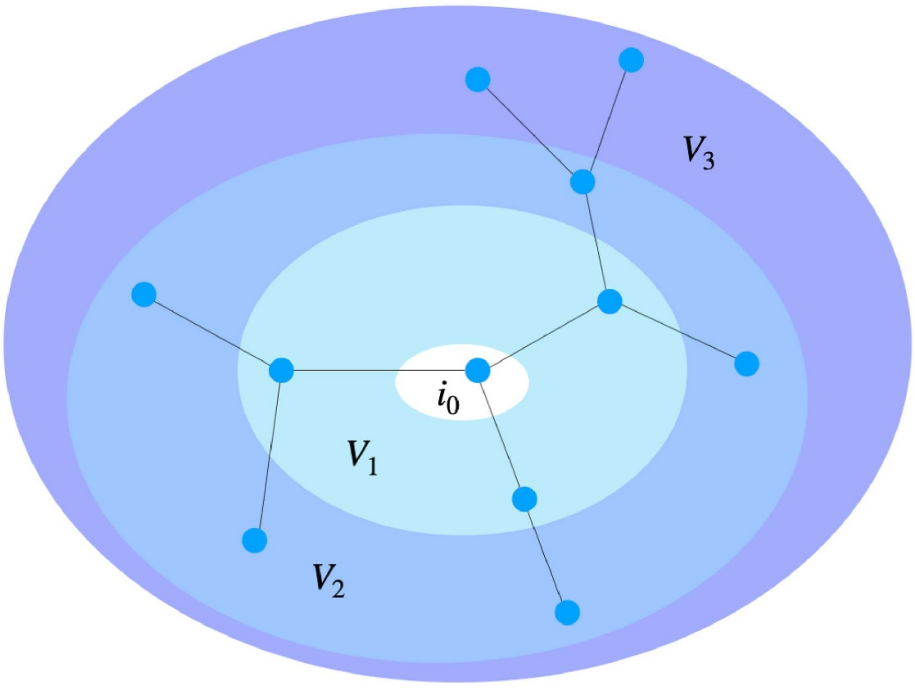

Figure B1. Illustration of the partitioning of nodes in a tree with root node i_0. The sets V_1, V_2, and V_3 contains nodes that are a distance 1, 2, are 3 separated from the root node i_0.

and determine the other nodes through a recursion. In particular, we set

$$\eta_{jj} = -\frac{M_{ij}}{M_{ji}}\eta_{ii}, \tag{B.7}$$

for $i \in V_k$ and $j \in V_{k+1}$. Since $M_{ij}M_{ji} < 0$, the elements $\eta_{ii} > 0$, and $\boldsymbol{\eta}$ is a symmetric, positive definite matrix. The procedure of constructing $\boldsymbol{\eta}$ is sketched in figure B1. Notice that the value of each element η_{ii} is determined by its path to the root node i_0, and this path is unique, as the graph is a tree.

Next, we show that

$$\mathbf{M}^T = -\boldsymbol{\eta}\mathbf{M}\boldsymbol{\eta}^{-1}, \tag{B.8}$$

so that $\mathbf{M}$ is strictly quasi-antisymmetric. Components wise, the right-hand side of equation (B.8) reads

$$-\left[\boldsymbol{\eta}\mathbf{M}\boldsymbol{\eta}^{-1}\right]_{ij} = \sum_{\ell=1}^{N}\sum_{k=1}^{N}\eta_{i\ell}M_{\ell k}\eta_{kj}^{-1} = \eta_{ii}M_{ij}\eta_{jj}^{-1}\,. \tag{B.9}$$

If $i = j$, or $i \neq j$ and the nodes are not each other's neighbours, then

$$-\left[\boldsymbol{\eta}\mathbf{M}\boldsymbol{\eta}^{-1}\right]_{ij} = -\eta_{ii}M_{ij}\eta_{jj}^{-1} = 0 = M_{ji}. \tag{B.10}$$

On the other hand, if $i \in V_k$ and $j \in V_{k+1}$, then equation (B.7) applies, and we obtain

$$-\left[\boldsymbol{\eta}\mathbf{M}\boldsymbol{\eta}^{-1}\right]_{ij} = -\eta_{ii}M_{ij}\eta_{jj}^{-1} = M_{ji}. \tag{B.11}$$

Equations (B.10) together with (B.11), imply equation (B.8), which is what we were meant to show.

Appendix C. Sign stability of antagonistic trees with nonzero diagonal elements

In appendix B, we have shown that all eigenvalues of the adjacency matrices of weighted, antagonistic tree matrices are purely imaginary. Now, we consider matrices of the form

$$\mathbf{M}' = \mathbf{M} - \mathbf{D} \tag{C.1}$$

where $\mathbf{M}$ is the adjacency matrix of a weighted, antagonistic tree as in appendix B, and $\mathbf{D}$ is a diagonal matrix with nonnegative diagonal entries, i.e. $[\mathbf{D}]_{ii} = D_{ii} \geqslant 0$. Hence, the distinction with the matrix $\mathbf{M}$ in

appendix B is that the diagonal entries of $\mathbf{M}'$ can be nonzero, and therefore for clarity we added the prime. We show that for this ensemble all eigenvalues have nonpositive real parts, i.e.

$$\Re\left[\lambda_i\left(\mathbf{M}'\right)\right] \leqslant 0 \tag{C.2}$$

for all $i = 1, 2, \ldots, N$.

The derivation consists of two parts. First, in section C.1, we perform a standard linear algebra computation to show that equation (C.2) holds for matrices $\mathbf{K}'$ built from subtracting a nonnegative diagonal matrix to an antisymmetric matrix. Second, in section C.2, we show that $\mathbf{M}'$ is related to a matrix $\mathbf{K}'$ by a similarity transformation, and hence they share the same eigenvalues. We end this appendix with a related result: in C.3 we show that the width spectrum of a diagonal matrix shrinks if we add to it an antisymmetric matrix.

C.1. Spectra of antisymmetric matrices with nonpositive diagonal entries

Let us consider matrices of the form

$$\mathbf{K}' = \mathbf{K} - \mathbf{D}, \tag{C.3}$$

where $\mathbf{K}$ is an antisymmetric matrix (instead of the adjacency matrix of an antagonistic tree in equation (C.1)), and where $\mathbf{D}$ is a nonnegative, diagonal matrix. We show that for matrices of this form,

$$\Re\left[\lambda_i\left(\mathbf{K}'\right)\right] \leqslant 0 \tag{C.4}$$

for all $i = 1, 2, \ldots, N$.

Indeed, in this case, for any vector $\vec{z} \in \mathbb{C}^N$, it holds that

$$\Re\left(\vec{z}^{\dagger}\,\mathbf{K}'\vec{z}\right) = \Re\left(\vec{z}^{\dagger}\,\mathbf{K}\vec{z}\right) - \Re\left(\vec{z}^{\dagger}\,\mathbf{D}\vec{z}\right) \leqslant 0. \tag{C.5}$$

As $[\mathbf{K}]_{jk} = -[\mathbf{K}]_{kj} \in \mathbb{R}$, it holds that

$$\sum_{k=1}^{N}\sum_{j=1}^{N} z_j^{*}\,[\mathbf{K}]_{jk}\,z_k = -\sum_{k=1}^{N}\sum_{j=1}^{N} z_j\,[\mathbf{K}]_{jk}\,z_k^{*}, \tag{C.6}$$

such that

$$\Re\left(\vec{z}^{\dagger}\,\mathbf{K}\vec{z}\right) = 0, \tag{C.7}$$

and

$$\vec{z}^{\dagger}\,\mathbf{D}\vec{z} = \sum_{j=1}^{N} |z_j|^2\,[\mathbf{D}]_{jj} \geqslant 0. \tag{C.8}$$

Using equations (C.7) and (C.8) in the left-hand side of (C.5), we obtain the right-hand side of equation (C.5). Lastly, to obtain the inequalities equation (C.4), we set $\vec{z}$ in equation (C.5) equal to a right eigenvector $\vec{r}_i$ of $\mathbf{K}'$, yielding,

$$\Re\left(\vec{r}_i^{\dagger}\mathbf{K}'\vec{r}_i\right) = \Re\left[\lambda_i\,|\vec{r}_i|^2\right] = |\vec{r}_i|^2\Re\left[\lambda_i\left(\mathbf{K}'\right)\right] \leqslant 0. \tag{C.9}$$

C.2. Antagonistic tree matrices with nonpositive diagonal entries

We show that antagonistic tree matrices $\mathbf{M}'$ with nonpositive diagonal entries, as defined in equation (C.1), are related by a similarity transformation to a matrix $\mathbf{K}'$ of the form equation (C.3). To this aim, we use $\boldsymbol{\eta}$ defined as in equations (B.6) and (B.7); notice that $\boldsymbol{\eta}$ is defined with $\mathbf{M}$ and not with $\mathbf{M}'$.

Indeed, if we define

$$\mathbf{K}' = \sqrt{\boldsymbol{\eta}}\mathbf{M}'\sqrt{\boldsymbol{\eta}}^{-1} \tag{C.10}$$

then

$$\mathbf{K}' = \mathbf{K} - \sqrt{\boldsymbol{\eta}}\mathbf{D}\sqrt{\boldsymbol{\eta}}^{-1} \tag{C.11}$$

with $\mathbf{K}$ the matrix as defined in equation (B.4), which is antisymmetric as we have shown in equation (B.5). Since the matrices $\sqrt{\boldsymbol{\eta}}$ and $\mathbf{D}$ are diagonal,

$$\sqrt{\boldsymbol{\eta}}\mathbf{D}\sqrt{\boldsymbol{\eta}}^{-1} = \mathbf{D} \tag{C.12}$$

and thus $\mathbf{K}'$ takes the form equation (C.3), as we were meant to show.

Since $\mathbf{M}'$ is related to $\mathbf{K}'$ by a similarity transformation, they share the same eigenvalues, and since $\mathbf{K}'$ has nonpositive eigenvalues, as we have shown in section C.1, also $\mathbf{M}'$ has nonpositive eigenvalues.

C.3. Change in the width of the spectrum after adding an antisymmetric or antagonistic tree matrix to a disordered diagonal matrix

Let $\mathbf{K}'$ be the sum of an antisymmetric matrix $\mathbf{K}$ and a (not necessarily nonpositive) diagonal matrix $-\mathbf{D}$, as defined in equation (C.3). It then holds that

$$\Re\left[\lambda_1\left(\mathbf{K}'\right)\right] \leqslant -D_{\min} \tag{C.13}$$

where $\lambda_1(\mathbf{K}')$ is the leading eigenvalue of the matrix $\mathbf{K}'$, and where $D_{\min}$ is the minimum entry of the D_i, as defined in equation (38). Analogously, it holds that

$$\Re\left[\lambda_N\left(\mathbf{K}'\right)\right] \geqslant -D_{\max}. \tag{C.14}$$

Equations (C.13) and (C.14) imply that the width of the spectrum of $-\mathbf{D}$ shrinks whenever an antisymmetric matrix is added to it, and hence adding antisymmetric interactions to a matrix makes it the matrix more stable. Note that this result does not extend to the more general case of sign-antisymmetric interactions, as then the matrix gets more stable in the perturbative regime of small interactions, but the matrix does not get more stable for strong sign-antisymmetric interactions, see [64].

The derivation of the equations (C.13) and (C.14) can be seen as an exercise is matrix analysis [71]. Nevertheless, for the reader's convenience, we present here a derivation. To derive equation (C.13), we consider the matrix

$$\mathbf{K}'' := \mathbf{K}' + D_{\min}\mathbf{1} = \mathbf{K} - \mathbf{D}' \tag{C.15}$$

where $\mathbf{D}' := \mathbf{D} - D_{\min}\mathbf{1}$ is by construction a diagonal matrix with nonnegative diagonal entries. Therefore, the results of C.2 apply to $\mathbf{K}''$, and

$$\Re\left[\lambda_1\left(\mathbf{K}''\right)\right] \leqslant 0. \tag{C.16}$$

Since,

$$\lambda_1\left(\mathbf{K}''\right) = \lambda_1\left(\mathbf{K}'\right) + D_{\min} \tag{C.17}$$

we obtain the equation (C.13) from combining equation (C.16) with (C.17).

Using a similar line of reasoning it follows that

$$\Re\left[\lambda_1\left(\mathbf{M}'\right)\right] \leqslant -D_{\min}, \tag{C.18}$$

where $\mathbf{M}'$ is now of the form equation (C.1) with $\mathbf{M}$ the adjacency matrix of a weighted, antagonistic tree and $\mathbf{D}$ a diagonal matrix with diagonal entries that can be negative and positive.

Appendix D. All the eigenvalues of the adjacency matrices of weighted, oriented graphs without directed cycles are equal to zero

Let $\mathbf{M} \in \mathbb{R}^{N\times N}$ represent the adjacency matrix of a weighted, directed graph. We assume that $M_{ii} = 0$, so that there are no self-links. If $M_{ij} = 0$, then the directed edge from i to j is absent, while if $M_{ij} \in \mathbb{R} \setminus 0$, then there exists a directed edge from i to j weighted by the value of M_{ij}.

We say that a directed graph is oriented if all of its edges are unidirectional, i.e.

$$M_{ij}M_{ji} = 0 \tag{D.1}$$

for all pairs of indices i, j. Additionally, we say that a graph has no directed cycles if equation (35) holds. Note that cycles that are nondirected, as for example the feedforward cycles in panel (c) of figure 1, are allowed.

The characteristic polynomial of an adjacency matrix of an oriented graph without directed cycles is given by

$$det(\lambda \mathbf{1} - \mathbf{M}) = \lambda^N, \tag{D.2}$$

and consequently all the eigenvalues of $\mathbf{M}$ are equal to zero, i.e.

$$\lambda_i(\mathbf{A}) = 0 \tag{D.3}$$

for all $i \in \{1, 2, \ldots, N\}$.

We show that equation (D.2) is true by identifying it as a specific case of the so-called Coefficients Theorem for directed graphs, which we revisit here. First, we present the Coefficients Theorem for unweighted graphs, i.e. for $M_{ij} \in \{0, 1\}$, which is theorem 1.2 in [70], and then we present the Coefficients Theorem for weighted graphs, i.e. for $M_{ij} \in \mathbb{R}$. Before stating the Coefficients Theorem, we need the following definition: A *linear directed graph* is a directed graph for which it holds that all vertices have an indegree and outdegree equal to one. Hence, linear directed graphs are composed out of one or more directed cycles.

Theorem 1 (Coefficients Theorem for directed graphs (Milic [88], Sachs [89], and Spialter [90])). *Let*

$$det(\lambda \mathbf{1} - \mathbf{M}) = \lambda^N + a_1 \lambda^{N-1} + \ldots + a_N \tag{D.4}$$

be the characteristic polynomial of an arbitrary directed graph G. Then

$$a_n = \sum_{L \in \mathcal{L}_n} (-1)^{p(L)}, \quad \text{with} \quad n = 1, 2, \ldots, N, \tag{D.5}$$

where $\mathcal{L}_n$ is the set of all linear directed subgraphs L of G with exactly n vertices; p(L) denotes the number of strongly connected components of L (i.e. the number of directed cycles of which L is composed).

Theorem 2 (Coefficients theorem for weighted directed graphs (Devadas Acharya [91])). *Let*

$$det(\lambda \mathbf{1} - \mathbf{M}) = \lambda^N + a_1 \lambda^{N-1} + \ldots + a_N \tag{D.6}$$

*be the characteristic polynomial of an arbitrary, weighted, directed graph with adjacency matrix **M**, then*

$$a_n = \sum_{L \in \mathcal{L}_n} (-1)^{p(L)} \prod_{(i,j) \in E(L)} M_{ij}, \quad \text{with} \quad n = 1, 2, \ldots, N, \tag{D.7}$$

where E(L) is the set of edges in the linear directed subgraph L.

In the case that G has no directed cycles, all coefficients a_i in Theorem 1 or Theorem 2 are equal to zero, and equation (D.2) follows as a corollary of the Coefficients Theorem for directed graphs.

Appendix E. Size dependence of the leading eigenvalues for different ensembles of sparse random matrices

In the figure E1 we show the leading eigenvalues shifted by their value at the smallest size and divided by the trend expected for the symmetric Erdős–Rényi ensemble [92]. The results for the antagonistic Erdős–Rényi ensemble shows an initial increase due to finite size effects and slight decay at large N, where the leading eigenvalue it is expected to saturate to a finite value. On the other hand, the results for the rescaled leading eigenvalues of the other ensembles are seen to increase at all the sizes observed.

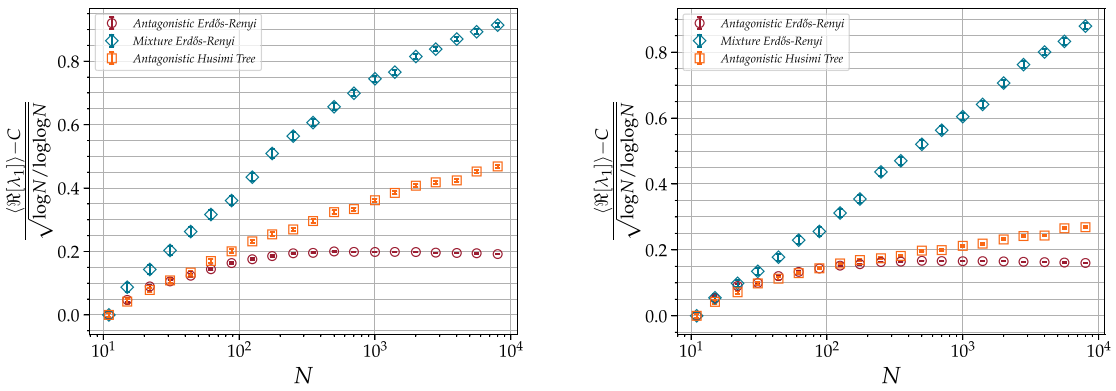

Figure E1. Average real part of the leading eigenvalue, $\langle \Re[\lambda_1] \rangle$ also shown in figures 5 and 7, here shifted by their value at the smallest size and by $\sqrt{\frac{\log N}{\log\log N}}$ expected in [92] for symmetric Erdős–Rényi graphs. Results shown are for antagonistic Erdős–Rényi graphs (red circles), mixture Erdős–Rényi graphs (blue diamonds) and antagonistic pure Husimi trees (orange squares).

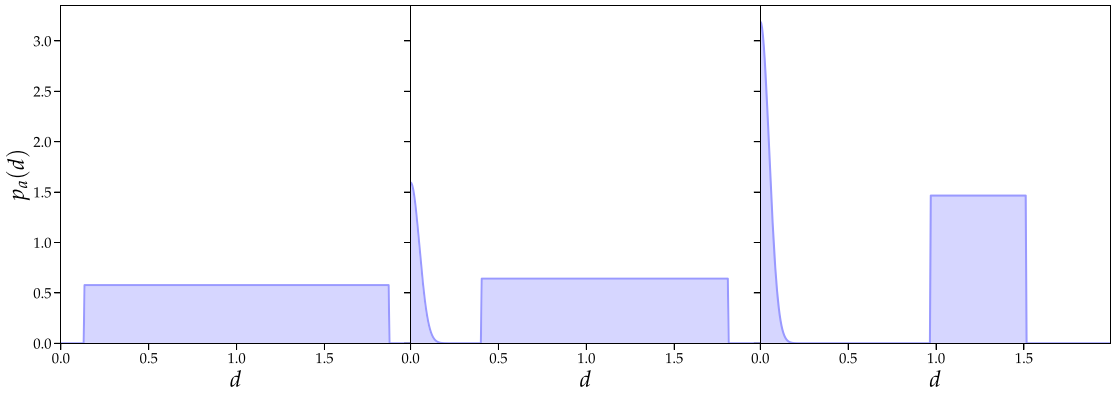

Figure F1. The distribution $p_a(d)$, as defined in appendix F, for three values of the parameter: $a = 0$ (left), $a = 0.1$ (centre) and $a = 0.2$ (right).

Appendix F. Husimi Plateau in Jacobian-like matrices

We refine the results in figure 7 by analysing $\langle \Re[\lambda_1(\mathbf{J})] \rangle$ as a function of N in the limit of $d_{\min} \approx 0$, where $d_{\min}$ is the smallest value of d that belongs to the support set of $p_D(d)$. In this limit, the leading eigenvalue of antagonistic, Husimi trees exhibits strong transient effects as a function of N, and hence it is important to carefully extrapolate the results to large N.

To study the influence of a value $d_{\min} \approx 0$ on the leading eigenvalue, we extract the diagonal entries D_i from a distribution $p_D(d) = p_a(d)$ that is plotted in figure F1. As illustrated by figure F1, the distribution $p_a(d)$ develops a peak around zero, i.e. $d \approx 0$, whose weight increases a function a, which is the main reason why we use $p_a(d)$ and not the uniform distribution considered before in figure 7. The distribution $p_a(d)$ is defined by

$$p_a(d) := a\, p_{\mathrm{HN}}(d) + (1-a)\, p_{\mathrm{U}}(d) \tag{F.1}$$

where $p_{\mathrm{HN}}(d)$ is a (narrow) half-normal distribution centred at zero, obtained by setting $\mu = 0$ and $\sigma = 0.05$ on the right-hand side of equation (24), and $p_{\mathrm{U}}(d)$ is a uniform distribution with a support that is not touching zero, and we denote its mean and standard deviation by μ_{U} and σ_{U}, respectively. We set the parameters μ_{U} and σ_{U} such that, as a varies, the first two cumulants of $p_a(d)$ are identical to those of $p_D(d)$ used in sections 4.2 and 4.3.

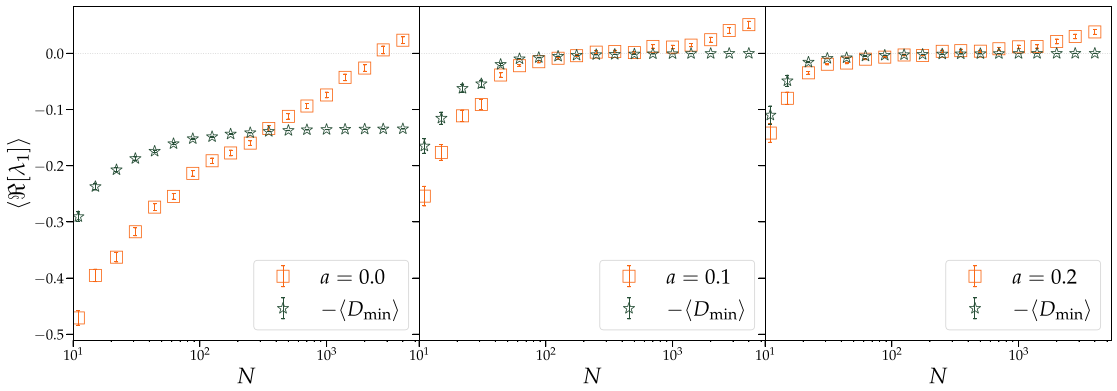

Figure F2. Average real part of the leading eigenvalue, $\langle \Re[\lambda_1] \rangle$, as a function of the matrix size N for Jacobian-like matrices $\mathbf{J}$ of antagonistic, Husimi trees. Numerical results obtained from diagonalising 300 matrix realisations of antagonistic Husimi trees (orange squares) are compared with the average of the largest element of the diagonal matrix $-D_{\min}$ (as defined in equation (38)), and error bars denote the error on the mean. The parameters used for the matrix ensembles are detailed in section 2.4.3, except for the distribution of diagonal elements which is given by $p_a(d)$, defined in equation (F.1).

Figure F2 plots $\langle \Re[\lambda_1(\mathbf{J})] \rangle$ as a function of N for antagonistic Husimi trees with diagonal elements drawn from $p_a(d)$ and for three values of a. In the left panel, the support of the diagonal distribution $p_a(d)$ does not include $d = 0$, and hence the functional behaviour of $\langle \Re[\lambda_1(\mathbf{J})] \rangle$ is analogous to the one shown in figure 7. On the other hand, in the middle and right panels $p_a(d)$ develops a peak around $d = 0$, and consequently the monotonic increase of $\langle \Re[\lambda_1(\mathbf{J})] \rangle$ as a function of N slows down significantly at intermediate values of N, leading to the appearance of a plateau. Note that the plateau is a transient effect, as for large enough values of N the steady increase of $\langle \Re[\lambda_1(\mathbf{J})] \rangle$ continues. Observe that increasing a only widens the plateau from the left side, making it appear at smaller sizes of fN. Hence, also when $p_a(d)$ is peaked around $d = 0$, $\langle \Re[\lambda_1(\mathbf{J})] \rangle$ diverges as a function of N, albeit with a strong, transient, plateau effect.

We end with some final remarks. Due to the Husimi plateau, we should carefully assess finite size effects in Husimi trees. In particular, we could wrongly conclude that $\langle \Re[\lambda_1] \rangle$ converges to a finite value when not considering large enough values of N. The Husimi plateau only occurs in Jacobian-like matrices if the support of the diagonal distribution contains $d = 0$, and hence we conjecture that it is related to the stripy structure of Jacobian-like matrices.

Appendix G. Finite size effect for the histograms of the imaginary part distribution of nonreal leading eigenvalues

In this appendix, we determine the effect of a finite size N on the distribution $p_{\Im[\lambda_1]}(x)$ plotted in figure 10. As we show, increasing the system size N, the discontinuity of the transition becomes more pronounced. Figure G1 plots the distribution $p_{\Im[\lambda_1]}(x)$ for different sizes N when the control parameter s is roughly at the transition s_{d} (in particular we set $s \simeq 0.08$, in correspondence with $\sigma_D = 0.10$, $\sigma_{\mathrm{G}} = 0.6$ and $\mu_{\mathrm{G}} = 1.0$).

As shown in figure G1, the typical value $\Im[\lambda_1^\star]$ of the distribution $p_{\Im[\lambda_1]}(x)$ presents in one instance only a very mild trend (although it is unclear whether it is statistically significant) due to finite size correction, still consistent with saturation to a finite value and therefore compatible with the discontinuous nature of the transition found in figure 10 and strongly supported by the reentrant behaviour of the support of the spectrum shown in figures 12 and 13. Interestingly, as the size N increases, the γ-distribution peaked at $\Im[\lambda_1^\star]$ gets more narrow, indicating that in the infinite size limit $\tilde{p}_{\Im[\lambda_1]}(x)$, as defined in equation (40), possibly converges to the delta distribution $\delta(x - \Im[\lambda_1^\star])$. Moreover, focusing on the behaviour of the nonreal histogram near the zero (see the insets in the top row of figure G1), we see find that the bin closest to the real delta peak decreases as a function of N, while the second bin increases as a function of N.

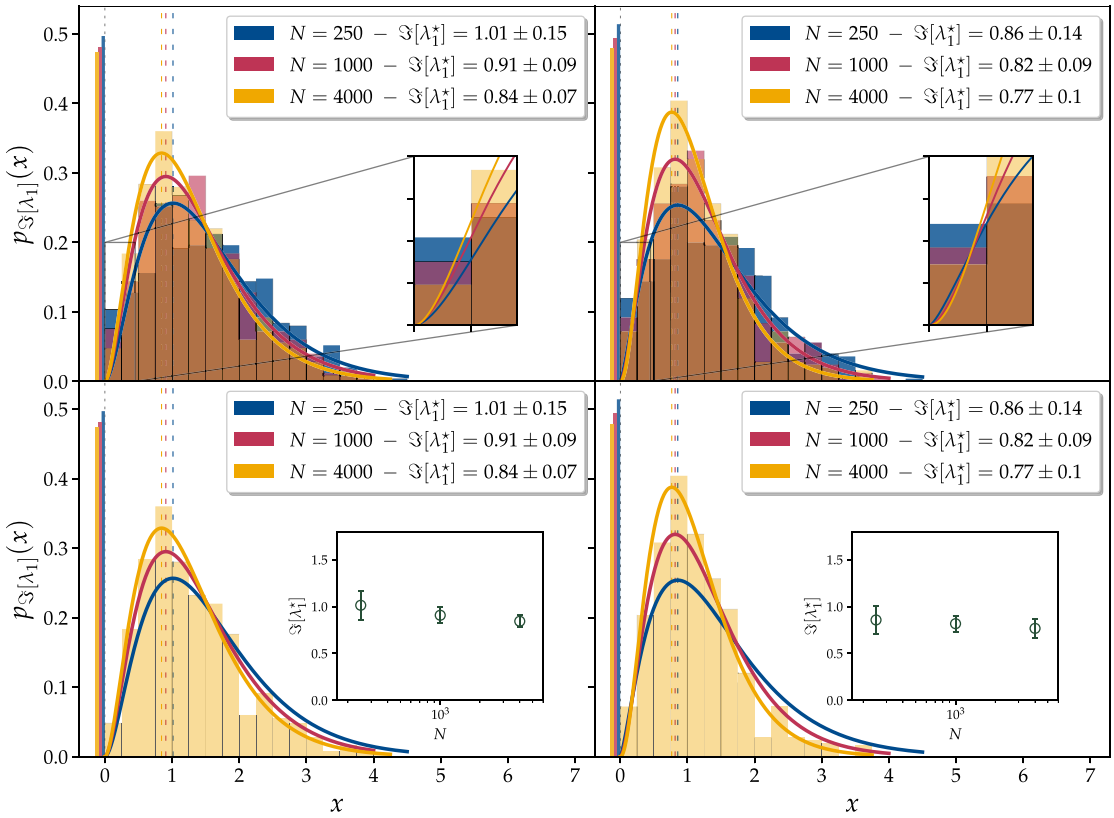

Figure G1. Histograms of the imaginary part of the leading eigenvalues of interaction-like (left panels) and Jacobian-like (right panels) matrices of antagonistic Erdös–Rényi graphs. The data shown corresponds with the parameter value $\sigma_D = 0.10$ at which the dynamical transition takes place in figure 10, albeit now for different matrix sizes N as indicated in the legend. Additionally, the insets show the histograms for the range $[0, 0.45]$ on the x-axis. The other parameters are the same as in figure 10. The figures at the bottom show, for reasons of clarity, the same data as the figures at the top, except for the absence of the histograms for $N = 250$ and $N = 1000$. The insets show the typical value of the leading eigenvalue imaginary part $\Im[\lambda_1^\star]$ as a function of N.

ORCID iDs

Pietro Valigi https://orcid.org/0009-0007-1593-1325
Izaak Neri https://orcid.org/0000-0001-9529-5742
Chiara Cammarota https://orcid.org/0000-0003-3443-6905

References

[1] May R M C 1973 *Stability and Complexity in Model Ecosystems (Monographs in Population Biology)* (Princeton University Press)
[2] Moore J C and de Ruiter P C 2012 *Energetic Food Webs: an Analysis of Real and Model Ecosystems* (Oxford University Press)
[3] Quirk J and Ruppert R 1965 Qualitative economics and the stability of equilibrium *Rev. Econ. Stud.* **32** 311–26
[4] Maybe J and Quirk J 1969 Qualitative problems in matrix theory *SIAM Rev.* **11** 30–51
[5] Sporns O 2016 *Networks of the Brain* (MIT Press)
[6] Clarke B L 1988 Stoichiometric network analysis *Cell Biophys.* **12** 237–53
[7] Angeli D 2009 A tutorial on chemical reaction networks dynamics *2009 European Control Conf. (ECC)* (IEEE) pp 649–57
[8] Cesari L 1963 *Asymptotic Behavior and Stability Problems in Ordinary Differential Equations* 2nd edn (Academic Inc.)
[9] Hahn W 1967 *Stability of Motion* (Springer)
[10] May R M C 1972 Will a large complex system be stable? *Nature* **238** 413–4
[11] Allesina S and Tang S 2015 The stability–complexity relationship at age 40: a random matrix perspective *Popul. Ecol.* **57** 63–75
[12] Rodgers G J and Bray A J 1988 Density of states of a sparse random matrix *Phys. Rev.* B **37** 3557–62
[13] Kühn R 2008 Spectra of sparse random matrices *J. Phys. A: Math. Theor.* **41** 295002
[14] Rogers T, Pérez Castillo I, Kühn R and Takeda K 2008 Cavity approach to the spectral density of sparse symmetric random matrices *Phys. Rev.* E **78** 031116
[15] Susca V A R, Vivo P and Kühn R 2021 Cavity and replica methods for the spectral density of sparse symmetric random matrices *SciPost Phys. Lect. Notes* 033
[16] Rogers T and Pérez Castillo I 2009 Cavity approach to the spectral density of non-hermitian sparse matrices *Phys. Rev.* E **79** 012101
[17] Lucas Metz F, Neri I and Bollé D'e 2011 Spectra of sparse regular graphs with loops *Phys. Rev.* E **84** 055101
[18] Bollé D'e, Lucas Metz F and Neri I 2013 On the spectra of large sparse graphs with cycles *Spectral Analysis, Differential Equations and Mathematical Physics: A Festschrift in Honor of Fritz Gesztesy's 60th Birthday* pp 35–58
[19] Neri I and Lucas Metz F L 2016 Eigenvalue outliers of non-hermitian random matrices with a local tree structure *Phys. Rev. Lett.* **117** 224101

[20] Lucas Metz F, Neri I and Rogers T 2019 Spectral theory of sparse non-hermitian random matrices *J. Phys. A: Math. Theor.* **52** 434003
[21] Neri I and Lucas Metz F 2020 Linear stability analysis of large dynamical systems on random directed graphs *Phys. Rev. Res.* **2** 033313
[22] Tarnowski W, Neri I and Vivo P 2020 Universal transient behavior in large dynamical systems on networks *Phys. Rev. Res.* **2** 023333
[23] Lucas Metz F and Neri I 2021 Localization and universality of eigenvectors in directed random graphs *Phys. Rev. Lett.* **126** 040604
[24] Tarnowski W 2022 Real spectra of large real asymmetric random matrices *Phys. Rev.* E **105** L012104
[25] Marcello Mambuca A, Cammarota C and Neri I 2022 Dynamical systems on large networks with predator-prey interactions are stable and exhibit oscillations *Phys. Rev.* E **105** 014305
[26] May R M 1973 Qualitative stability in model ecosystems *Ecology* **54** 638–41
[27] Jeffries C 1974 Qualitative stability and digraphs in model ecosystems *Ecology* **55** 1415–9
[28] Levins R 1975 Problems of signed digraphs in ecological theory *Ecosystem Analysis and Prediction. Society for Industrial and Applied Mathematics, Philadelphia* pp 264–77
[29] Solimano F and Beretta E 1982 Graph theoretical criteria for stability and boundedness of predator-prey systems *Bull. Math. Biol.* **44** 579–85
[30] Logofet D O and Ulianov N B 1982 Sign stability in model ecosystems: a complete class of sign-stable patterns *Ecol. Modelling* **16** 173–89
[31] Clarke B L 1975 Theorems on chemical network stability *J. Chem. Phys.* **62** 773–5
[32] Jeffries C, Klee V and Van den Driessche P 1977 When is a matrix sign stable? *Can. J. Math.* **29** 315–26
[33] Mézard M and Parisi G 2001 The Bethe lattice spin glass revisited *Eur. Phys. J.* B **20** 217–33
[34] Dembo A and Montanari A 2010 Gibbs measures and phase transitions on sparse random graphs *Braz. J. Probab. Stat.* **24** 137–211
[35] Montanari A, Mossel E and Sly A 2012 The weak limit of Ising models on locally tree-like graphs *Probab. Theory Relat. Fields* **152** 31–51
[36] Jacquet C, Moritz C, Morissette L, Legagneux P, Massol F, Archambault P and Gravel D 2016 No complexity–stability relationship in empirical ecosystems *Nat. Commun.* **7** 1–8
[37] Arnold V I 1992 *Ordinary Differential Equations* (Springer Science & Business Media) ch 3
[38] Hirsch M W, Smale S and Devaney R L 2012 *Differential Equations, Dynamical Systems and an Introduction to Chaos* (Academic) ch 6
[39] Dorogovtsev S N and Mendes J F F 2022 *The Nature of Complex Networks* (Oxford University Press)
[40] Sompolinsky H, Crisanti A and Sommers H J 1988 Chaos in random neural networks *Phys. Rev. Lett.* **61** 259–62
[41] Kadmon J and Sompolinsky H 2015 Transition to chaos in random neuronal networks *Phys. Rev.* X **5** 041030
[42] Guo Y and Amir A 2021 Exploring the effect of network topology, mrna and protein dynamics on gene regulatory network stability *Nat. Commun.* **12** 1–10
[43] Moran J and Bouchaud J-P 2019 May's instability in large economies *Phys. Rev.* E **100** 032307
[44] François Verhulst P 1845 Resherches mathematiques sur la loi d'accroissement de la population *Nouveaux Memoires de l'Academie Royale des Sciences* **18** 1–41
[45] Volterra V 1926 Fluctuations in the abundance of a species considered mathematically *Nature* **118** 558–60
[46] Barbier M, Arnoldi J-F, Bunin G and Loreau M 2018 Generic assembly patterns in complex ecological communities *Proc. Natl Acad. Sci.* **115** 2156–61
[47] Rossberg A G 2013 *Food Webs and Biodiversity: Foundations, Models, Data* (Wiley)
[48] Dougoud M, Vinckenbosch L, Rohr R P, Bersier L-F and Mazza C 2018 The feasibility of equilibria in large ecosystems: a primary but neglected concept in the complexity-stability debate *PLoS Comput. Biol.* **14** e1005988
[49] Roberts A 1974 The stability of a feasible random ecosystem *Nature* **251** 607–8
[50] Meszéna G, Gyllenberg M, Pásztor L and Metz J A J 2006 Competitive exclusion and limiting similarity: a unified theory *Theor. Popul. Biol.* **69** 68–87
[51] Shear McCann K 2000 The diversity–stability debate *Nature* **405** 228–33
[52] Mougi A and Kondoh M 2012 Diversity of interaction types and ecological community stability *Science* **337** 349–51
[53] Rossberg A G, Caskenette A L and Bersier L-F 2017 Structural instability of food webs and food-web models and their implications for management *Adaptive Food Webs: Stability and Transitions of Real and Model Ecosystems* pp 373–83
[54] Rohr R P, Saavedra S and Bascompte J 2014 On the structural stability of mutualistic systems *Science* **345** 6195
[55] Biroli G, Bunin G and Cammarota C 2018 Marginally stable equilibria in critical ecosystems *New J. Phys.* **20** 083051
[56] O'Sullivan J D, Knell R J and Rossberg A G 2019 Metacommunity-scale biodiversity regulation and the self-organised emergence of macroecological patterns *Ecol. Lett.* **22** 1428–38
[57] Garcia Lorenzana G and Altieri A 2022 Well-mixed Lotka-Volterra model with random strongly competitive interactions *Phys. Rev.* E **105** 024307
[58] Grilli J, Adorisio M, Suweis S, Barabás G, Banavar J R, Allesina S and Maritan A 2017 Feasibility and coexistence of large ecological communities *Nat. Commun.* **8** 1–8
[59] Stephens P A, Sutherland W J and Freckleton R P 1999 What is the Allee effect? *Oikos* **87** 185–90
[60] Stone L 2018 The feasibility and stability of large complex biological networks: a random matrix approach *Sci. Rep.* **8** 1–12
[61] Allesina S and Tang S 2012 Stability criteria for complex ecosystems *Nature* **483** 205–8
[62] Marcus S, Turner A M and Bunin G 2022 Local and collective transitions in sparsely-interacting ecological communities *PLoS Comput. Biol.* **18** e1010274
[63] Bianconi G and Marsili M 2005 Loops of any size and hamilton cycles in random scale-free networks *J. Stat. Mech.* 06005
[64] Cure S and Neri I 2023 Antagonistic interactions can stabilise fixed points in heterogeneous linear dynamical systems *SciPost Phys.* **14** 093
[65] Erdős P and Rényi A 1959 On random graphs I *Publicationes Math.* **64** 290–7
[66] Bollobás B 2001 *Random Graphs* (*Cambridge Studies in Advanced Mathematics*) 2nd edn (Cambridge University Press) p 73
[67] Harary F and Uhlenbeck G E 1953 On the number of Husimi trees: I *Proc. Natl Acad. Sci.* **39** 315–22
[68] Husimi K 1950 Note on Mayers' theory of cluster integrals *J. Chem. Phys.* **18** 682–4
[69] Yamada T 1987 Generic matrix sign-stability *Can. Math. Bull.* **30** 370–6
[70] Sachs H, Doob M and Cvetkovic D M 1979 *Spectra of Graphs: Theory and Applications* (VEB Deutscher Verlag der Wissenschaften
[71] Horn R A and Johnson C R 2013 *Matrix Analysis* 2nd edn (Cambridge University Press)
[72] Krivelevich M and Sudakov B 2003 The largest eigenvalue of sparse random graphs *Comb. Probab. Comput.* **12** 61–72
[73] Chung F, Linyuan L and Van V 2004 The spectra of random graphs with given expected degrees *Internet Math.* **1** 257–75

[74] Gibbs T, Grilli J, Rogers T and Allesina S 2018 Effect of population abundances on the stability of large random ecosystems *Phys. Rev.* E **98** 022410
[75] Wilson E B 1927 Probable inference, the law of succession and statistical inference *J. Am. Stat. Assoc.* **22** 209–12
[76] Agresti A and Coull B 1998 Approximate is better than 'exact' for interval estimation of binomial proportions *Am. Stat.* **52** 119–26
[77] Brown L D, Tony Cai T and DasGupta A 2001 Interval estimation for a binomial proportion *Stat. Sci.* **16** 101–33
[78] Neutel A-M and Thorne M A S 2014 Interaction strengths in balanced carbon cycles and the absence of a relation between ecosystem complexity and stability *Ecol. Lett.* **17** 651–61
[79] Roy F, Biroli G, Bunin G and Cammarota C 2019 Numerical implementation of dynamical mean field theory for disordered systems: application to the Lotka-Volterra model of ecosystems *J. Phys. A: Math. Theor.* **52** 484001
[80] Roy F, Barbier M, Biroli G and Bunin G 2020 Complex interactions can create persistent fluctuations in high-diversity ecosystems *PLoS Comput. Biol.* **16** e1007827
[81] Bunin G 2017 Ecological communities with Lotka-Volterra dynamics *Phys. Rev.* E **95** 042414
[82] Pearce M T, Agarwala A and Fisher D S 2020 Stabilization of extensive fine-scale diversity by ecologically driven spatiotemporal chaos *Proc. Natl Acad. Sci.* **117** 14572–83
[83] Dunne J A, Williams R J and Martinez N D 2002 Food-web structure and network theory: the role of connectance and size *Proc. Natl Acad. Sci.* **99** 12917–22
[84] Neutel A-M, Heesterbeek J A P and De Ruiter P C 2002 Stability in real food webs: weak links in long loops *Science* **296** 1120–3
[85] Joglekar Y N and Karr W A 2011 Level density and level-spacing distributions of random, self-adjoint, non-hermitian matrices *Phys. Rev.* E **83** 031122
[86] Feinberg J and Riser R 2022 Pseudo-hermitian random matrix models: General formalism *Nucl. Phys.* B **975** 115678
[87] Bender C M, Boettcher S and Meisinger P N 1999 Pt-symmetric quantum mechanics *J. Math. Phys.* **40** 2201–29
[88] Milic M 1964 Flow-graph evaluation of the characteristic polynomial of a matrix *IEEE Trans. Circuit Theory* **11** 423–4
[89] Sachs H 1964 Beziehungen zwischen den in einem graphen enthaltenen kreisen und seinem charakteristischen polynom *Publ. Math. Debrecen* **11** 119–34
[90] Spialter L 1964 The atom connectivity matrix characteristic polynomial (acmcp) and its physico-geometeric (topological) significance *J. Chem. Doc.* **4** 269–74
[91] Devadas Acharya B 1980 Spectral criterion for cycle balance in networks *J. Graph Theory* **4** 1–11
[92] Benaych-Georges F, Bordenave C and Knowles A 2019 Largest eigenvalues of sparse inhomogeneous Erdős–Rényi graphs *Ann. Probab.* **47** 1653–76